Published OnlineFirst March 29, 2013; DOI: 10.1158/0008-5472.CAN-12-4136

Molecular and Cellular Pathobiology

Cancer Research

Acquired Resistance to EGFR Inhibitors Is Associated with a Manifestation of Stem Cell–like Properties in Cancer Cells

Kazuhiko Shien[1], Shinichi Toyooka[1], Hiromasa Yamamoto[1], Junichi Soh[1], Masaru Jida[1], Kelsie L. Thu[4], Shinsuke Hashida[1], Yuho Maki[1], Eiki Ichihara[2], Hiroaki Asano[1], Kazunori Tsukuda[1], Nagio Takigawa[3], Katsuyuki Kiura[2], Adi F. Gazdar[5], Wan L. Lam[4], and Shinichiro Miyoshi[1]

Abstract

Acquired resistance to EGF receptor (EGFR) tyrosine kinase inhibitor (TKI) is a critical problem in the treatment of lung cancer. Although several mechanisms have been shown to be responsible for acquired resistance, all mechanisms have not been uncovered. In this study, we investigated the molecular and cellular profiles of the acquired resistant cells to EGFR-TKI in *EGFR*-mutant lung cancers. Four *EGFR*-mutant cell lines were exposed to gefitinib by stepwise escalation and high-concentration exposure methods, and resistant sublines to gefitinib were established. The molecular profiles and cellular phenotypes of these resistant sublines were characterized. Although previously reported, alterations including secondary *EGFR* T790M mutation, *MET* amplification, and appearance of epithelial-to-mesenchymal transition (EMT) features were observed, these 2 drug-exposure methods revealed different resistance mechanisms. The resistant cells with EMT features exhibited downregulation of miRNA-200c by DNA methylation. Furthermore, the HCC827-derived subline characterized by the high-concentration exposure method exhibited not only EMT features but also stem cell–like properties, including aldehyde dehydrogenase isoform 1 (ALDH1A1) overexpression, increase of side-population, and self-renewal capability. Resistant sublines with stem cell–like properties were resistant to conventional chemotherapeutic agents but equally sensitive to histone deacetylase and proteasome inhibitors, compared with their parental cells. ALDH1A1 was upregulated in clinical samples with acquired resistance to gefitinib. In conclusion, our study indicates that the manner of EGFR-TKI exposure influences the mechanism of acquired resistance and the appearance of stem cell–like property with EGFR-TKI treatment. *Cancer Res; 73(10); 1–11. ©2013 AACR.*

Introduction

EGF receptor (*EGFR*) mutations are oncogenic alterations in non–small cell lung carcinoma (NSCLC; refs. 1, 2). First-generation EGFR-tyrosine kinase inhibitors (TKI), such as gefitinib and erlotinib, have exhibited significant antiproliferative effects against NSCLC with *EGFR* mutations in preclinical studies (1, 2) and have also resulted in prolonged disease-free survival in randomized phase III studies (3–5). However, patients with *EGFR*-activating mutations who initially respond to EGFR-TKIs eventually acquire resistance, which is a critical problem in the treatment of patients with advanced NSCLC. Several mechanisms are believed to be responsible for acquired resistance to EGFR-TKI, including secondary *EGFR* T790M and minor mutations, *MET* amplification, and activation of MET/HGF axis, acquiring an epithelial-to-mesenchymal transition (EMT) signature, and transformation from NSCLC into small cell lung cancer (SCLC; refs. 6–11). More recently, AXL kinase activation and loss of the *EGFR*-mutant allele have been reported as possible mechanisms of resistance, but it is likely that additional mechanisms remain to be identified (12, 13).

Establishment of resistant sublines is a common experimental method to investigate the mechanism of drug resistance. The properties of resistant cells can vary according to the experimental methods used in the developing process. For example, in endometrial cancer, cisplatin-resistant cells established by stepwise escalation exposure and high-concentration exposure methods showed different cellular properties that may be either a cause or result of drug resistance (14). This fact suggests that the mechanism of EGFR-TKI resistance may vary according to *in vitro* culture

Authors' Affiliations: Departments of [1]Thoracic Surgery and [2]Respiratory Medicine, Okayama University Hospital; [3]Department of General Internal Medicine 4, Kawasaki Medical School, Okayama, Japan; [4]Department of Integrative Oncology, British Columbia Cancer Research Centre, Vancouver, British Columbia, Canada; and [5]Hamon Center for Therapeutic Oncology Research and Department of Pathology, University of Texas Southwestern Medical Center, Dallas, Texas

Note: Supplementary data for this article are available at Cancer Research Online (http://cancerres.aacrjournals.org/).

Corresponding Author: Shinichi Toyooka, Department of Thoracic Surgery, Okayama University Hospital, 2-5-1 Shikata-cho, Kita-ku, Okayama 700-8558, Japan. Phone: 81-86-235-7265; Fax: 81-86-235-7269; E-mail: toyooka@md.okayama-u.ac.jp

doi: 10.1158/0008-5472.CAN-12-4136

Published OnlineFirst March 29, 2013; DOI: 10.1158/0008-5472.CAN-12-4136

conditions, resulting in finding of novel features of resistant cells. Although the majority of previously reported cells that were resistant to EGFR-TKI were established with stepwise escalation of EGFR-TKI concentration, we successfully established resistant cells with the high-concentration exposure method as well as the stepwise escalation method, and identified novel features of cells resistant to EGFR-TKI. The purposes of this study were to investigate the acquired mechanism of resistance to EGFR-TKI and to explore strategies to overcome resistance to EGFR-TKI.

Materials and Methods

Cell lines and reagents

EGFR-mutant HCC827 (exon19del E746–A750), PC-9 (exon19del E746–A750), HCC4006 (exon19del L747–E749), and HCC4011 (L858R) cells were used. These cell lines except for PC-9 were established by one of the authors (A.F. Gazdar). PC-9 was obtained from Immuno-Biological Laboratories. All the cell lines were cultured in RPMI-1640 media supplemented with 10% FBS, and grown in a humidified incubator with 5% CO_2 at 37°C. EGFR-TKI–resistant sublines were established by 2 different methods: parental cells were cultured with stepwise escalation of concentrations of gefitinib from 5 nmol/L to 2 μmol/L over 6 months (stepwise escalation method), or initially high concentration of gefitinib (2 μmol/L) over 6 months (high-concentration method). Finally, gefitinib-resistant sublines named as HCC827-GR-step, PC-9-GR-step, HCC4006-GR-step, and HCC4011-GR-step were established by stepwise escalation method, and HCC827-GR-high1, HCC827-GR-high2, PC-9-GR-high, HCC4006-GR-high, and HCC4011-GR-high were established by high-concentration method. About HCC827-GR-high1 and high2, these 2 sublines were independently established from different cultures with high-concentration method. The identities of all the parental and resistant cells were confirmed by analyzing the short tandem repeat profile using the Cell ID System (Promega) and ABI Prism 310 Genetic Analyzer (Applied Biosystems), according to the manufacturer's instructions. Clonal-resistant cells were isolated by limiting dilution.

Details about the reagents used in the cell proliferation assay and the antibodies for Western blot analysis, fluorescence immunocytochemistry, and immunohistochemistry are included in the Supplementary Methods.

Determination of cell proliferation

Cell proliferation was determined by a modified MTS assay with CellTiter 96 AQueous One Solution Reagent (Promega) as previously reported (15). The antiproliferative effects are shown as IC_{50}, which is the concentration of the drug required to inhibit cell proliferation by 50%.

Western blot analysis

The detailed protocol for the Western blotting has been described previously (15). Monoclonal antiactin antibody, used as an equal loading control, was purchased from Merch KGaA. The following secondary antibodies were used: goat anti-rabbit or anti-mouse immunoglobulin G (IgG)-conjugated horseradish peroxidase (Santa Cruz Biotechnology). To detect specific signals, the membranes were examined using ECL Prime Western Blotting Detection System (GE Healthcare).

Phospho-receptor tyrosine kinase array and phospho-kinase arrays

A Human Phospho-Receptor Tyrosine Kinase (RTK) Array Kit and a Human Phospho-Kinase Array Kit (R&D Systems) were used to measure the relative level of tyrosine phosphorylation of 42 distinct RTKs and the relative level of phosphorylation of 46 distinct intracellular kinases. Both arrays were conducted according to the manufacturer's instructions.

Fluorescence immunocytochemistry

The cells were cultured and fixed by 4% formaldehyde on chamber slides. Primary antibodies against EGFR, E-cadherin, vimentin, aldehyde dehydrogenase isoform 1 (ALDH1A1), and ABCB1 were used. Further details are provided in the Supplementary Methods.

DNA and RNA extraction

Genomic DNAs were isolated from cell lines, frozen tumors, or paraffin-embedded tumor by using DNeasy Blood and Tissue Kit (Qiagen), standard phenol–chloroform (1:1) extraction followed by ethanol precipitation, or QIAmp DNA FFPE Tissue Kit (Qiagen), respectively. Total RNAs were extracted from cell lines using RNeasy Plus Mini Kit (Qiagen). The cDNA was synthesized from total RNA using High-Capacity cDNA Reverse Transcription Kits (Applied Biosystems) according to the manufacturer's instructions.

Direct sequencing, PCR-based length polymorphism assay, and subcloning

We determined the mutational status of *EGFR*, *KRAS*, *NRAS*, and *BRAF* genes by direct sequencing, and PCR conditions are provided in Supplementary Table S1A. *EGFR* exon 19 deletion was also detected with PCR-based length polymorphism assay, which have previously reported (16). For subcloning, PCR products were cloned into pCR2.1-TOPO vector using TOPO TA Cloning Kit (Invitrogen). One hundred clones were randomly selected for PCR-based length polymorphism assay.

Analyses of copy number by qPCR and FISH assays

Copy number gains (CNG) of *EGFR* and *MET* genes were determined by quantitative real-time PCR (qPCR) assay using Power SYBR Green PCR Master Mix (Applied Biosystems), as previously reported (17, 18). Primer sequences are provided in Supplementary Table S1B. In brief, gene dosage of each target and *LINE-1* gene, a reference gene, was calculated using the standard curve method. Relative copy number of each sample was determined by comparing the ratio of target gene to *LINE-1* in each sample with the ratio of these genes in human genomic DNA (EMD Biosciences). On the basis of our previous study, we defined high-level amplification as values greater than 4 in cell lines and those greater than 5 in clinical samples (17, 18).

A dual-color FISH assay was conducted using the LSI EGFR SpectrumOrange/CEP7 SpectrumGreen probe (Vysis)

Published OnlineFirst March 29, 2013; DOI: 10.1158/0008-5472.CAN-12-4136

according to the manufacturer's instructions. Twenty metaphase spreads and 200 interphase nuclei were analyzed in each slide.

Hybridoma production and TKI sensitivity analysis

The parental HCC827 cells were fused with HCC827-GR-high2 using Sendai virus (hemagglutinating virus of Japan) envelope (HVJ-E) GenomONE-CF (Ishihara Sangyo Kaisha Ltd.) according to the manufacturer's instructions. In brief, HCC827 cells stained with PKH26 Red fluorescent Cell Linker Kit (Sigma-Aldrich) were mixed at a ratio of 1:1 HCC827-GR-high2 cells stained with PKH67 Green fluorescent Cell Linker Kit (Sigma-Aldrich). The fused cells were confirmed as double-fluorescent positive cells in fluorescent microscopy. Cells were treated with 2 μmol/L of gefitinib and the presence of double-fluorescent positive and single-fluorescent positive cells (HCC827 and HCC827-GR-high2) was examined 14 days after.

Expression profiling analysis

RNA from cells was profiled on Illumina HumanHT-12 V4 Expression BeadChip arrays according to the Illumina protocol. The array measures expression levels for more than 47,000 transcripts derived from the NCBI RefSeq Release 38. BRB array tools (version 4.2) were used to conduct robust spline normalization on background corrected data to generate $\log_2$-transformed normalized data. Fold change in expression for individual probes was calculated and probes with fold changes exceeding 2-fold or below 2-fold were considered over- and underexpressed, respectively (Supplementary Table S2).

mRNA and miRNA expression analysis by qRT-PCR

mRNA expression analysis by quantitative reverse transcription PCR (qRT-PCR) was conducted on cDNA using TaqMan probes and the TaqMan Universal PCR Master Mix (Applied Biosystems). In miRNA expression analysis, the miRNA was isolated with TaqMan MicroRNA Cells-to-CT Kit (Ambion), and reverse transcription was conducted with TaqMan MicroRNA Reverse Transcriptional Kit systems (Applied Biosystems) using TaqMan primers for each miRNA. Primer and probe sets (Supplementary Table S1C and S1D) were purchased from Applied Biosystems and used according to manufacturer's instructions. PCR amplification was conducted on an ABI StepOne Real-Time PCR Instrument (Applied Biosystems) and gene expression was calculated using the comparative C_T method. Three replicates per sample were assayed for each gene. To quantify the relative changes in gene expression, the 2 $(-\Delta\Delta C_T)$ method was used and reactions were normalized to endogenous control gene glyceraldehyde-3-phosphate dehydrogenase (*GAPDH*) expression levels in mRNA expression analysis, and miR-374 expression level in miRNA expression analysis, respectively.

DNA methylation analysis

DNA was subjected to bisulfate treatment using Epitect Bisulfite Kit (Qiagen) according to the manufacturer's protocol. DNA methylation status was examined by bisulfite genomic sequencing and methylation-specific PCR (MSP) as previously reported (19). Primers are listed in Supplementary Table S1E and S1F.

Sphere formation assays in serum-free cultures

A total of 5×10^3 of cells were plated in 24-well plates with Ultra-Low Attachment surface (Corning Inc.), and cultured in serum-free Dulbecco's Modified Eagle Medium F12 (Invitrogen) supplemented with 20 ng/mL EGF and 10 ng/mL basic fibroblast growth factor (bFGF; all from Sigma-Aldrich). The numbers of spheres exceeding 150 μm in size for each well were counted by microscope after 14 days of culturing.

Side-population analysis

The basic protocol for side-population analysis was based on Goodell and colleagues (20). Cells were resuspended at 1×10^6/mL in prewarmed RPMI-1640, and Hoechst 33342 dye (Sigma-Aldrich) was added to a final concentration of 5 μg/mL in the presence or absence of verapamil (30 μg/mL; Sigma-Aldrich). The cells were then incubated at 37°C for 75 minutes with intermittent shaking. Propidium iodide (Sigma-Aldrich) was added to the cells, to a final concentration of 1 μg/mL, to gate the viable cells. The cell preparations were filtered through a 40-mm cell strainer to obtain single cell suspension. The cell samples were then analyzed on a BD FACSVantage SE (BD Biosciences) cell sorter. The side population was identified as a group of cells that did not take up the Hoechst dye, a characteristic abolished with verapamil treatment (20). These analyses were conducted at ReproCELL.

Tumor cell implantation experiments

HCC827, HCC827-GR-high1, and HCC827-GR-high2 cells were subcutaneously injected into the nonobese diabetic/severe combined immunodeficient (NOD/SCID) mice purchased from Charles River. Groups of mice were inoculated with each cell line at 5×10^6. Tumor growth was monitored and individual tumor volumes were measured using a digital caliper and approximated according to the formula $V = 1/2ab^2$ (a, the long diameter and b, the short diameter of the tumor). At the end of experiments, mice were sacrificed after 4 weeks and tumors were harvested, measured, photographed, and pathologically examined.

Immunothistochemical anaylses of clinical samples

Tumor samples were obtained at Okayama University Hospital (Okayama, Japan) with patients' consent under Institutional Review Board–approved protocols. Biopsied samples after acquisition of EGFR-TKI resistance were fixed in 10% formaldehyde and embedded in paraffin. Immunohistochemical (IHC) staining with ALDH1A1 (diluted 1:400 in PBS), ABCB1 (1:200), E-cadherin (1:1,000), and vimentin (1:200) was conducted. The detailed protocol for the IHC staining has been described previously (21).

Statistical analyses

All data were analyzed using JMP v 9.0.0 software (SAS Institute Inc.). $P < 0.05$ was considered significant. All tests were two-sided.

Published OnlineFirst March 29, 2013; DOI: 10.1158/0008-5472.CAN-12-4136

Results

Genotypic mechanisms of acquired resistance to EGFR-TKIs

Four cell lines (HCC827, PC-9, HCC4006, and HCC4011) with TKI-sensitive *EGFR* mutations were exposed to gefitinib by 2 different methods: stepwise escalation (GR-step series) and high-concentration exposure (GR-high series). From these efforts, 9 sublines resistant to gefitinib were established: HCC827-GR-step, PC-9-GR-step, HCC4006-GR-step, HCC4011-GR-step, HCC827-GR-high1, HCC827-GR-high2, PC-9-GR-high, HCC4006-GR-high, and HCC4011-GR-high. The IC_{50} values against gefitinib and erlotinib of these 9 resistant sublines exceeded 5 μmol/L (Table 1). The expressions of EGFR and its effector proteins in these cell lines were profiled (Supplementary Fig. S1A). To explore the genotypic changes following acquired resistance to EGFR-TKIs, we examined the genomic DNA of both parental and resistant cells. In sublines established with the stepwise escalation method, qPCR revealed that HCC827-GR-step and HCC4011-GR-step exhibited *MET* amplification (Supplementary Fig. S1B), whereas PC-9-GR-step showed the presence of *EGFR* T790M mutation detected by direct sequencing (Supplementary Fig. S1C). Among sublines established with the high-concentration method, only HCC4011-GR-high showed *MET* amplification (Supplementary Fig S1B). These resistance mechanisms were consistent with the results of previous studies (22–24). Neither T790M nor *MET* amplification was observed in any of the other 5 sublines (HCC4006-GR-step, HCC827-GR-high1, HCC827-GR-high2, PC-9-GR-high, and HCC4006-GR-high). No resistant sublines harbored secondary mutations in the *KRAS*, *NRAS*, or *BRAF* gene.

After acquiring resistance to EGFR-TKIs, all sublines except HCC827-GR-high2 retained *EGFR* mutations, CNG, and protein expression, as determined by direct sequencing, qPCR, and Western blotting, respectively (Supplementary Fig. S1). Originally, parental HCC827 cells showed focal amplification of *EGFR* with 32.3 copies estimated by FISH and qPCR assays. In HCC827-GR-high2, qPCR, PCR-based length polymorphism and FISH assays revealed progressive decrease in the *EGFR*-mutant allele through the course of passages leading to the disappearance of focally amplified *EGFR* alleles (Fig. 1). Subcloning of the PCR product from HCC827-GR-high2 produced 100 of 100 clones exhibiting wild-type *EGFR* instead of the exon 19 deletion, as determined by PCR-based length polymorphism assay. In addition, 3 sublines from independent single cells were established from HCC827-GR-high2. No mutant alleles were detected in 2 of these sublines, whereas a small population of mutant alleles was identified in the third subline as determined by direct sequencing. These data indicate that the focal amplification of the *EGFR* gene, which was considered a mutant allele, disappeared in HCC827-GR-high2.

Phenotypic change in acquiring resistance

Microscopically, each of the 4 sublines, HCC827-GR-high1, HCC827-GR-high2, HCC4006-GR-high, and HCC4006-GR-step, exhibited a spindle cell–like morphology that was different from their parental cell lines. As expected, these 4 sublines displayed EMT features in Western blotting and fluorescence immunocytochemistry for E-cadherin and vimentin (Supplementary Fig. S2A and S2B). In contrast, PC-9 and HCC4011 cells and the derived resistant sublines did not show EMT features.

Expression profile of mRNA and kinases in HCC827 cells

Because we had a great interest in HCC827-GR-high2 whose amplified *EGFR*-mutant alleles disappeared, we examined the mRNA expression profile in HCC827-GR-high2 by using cDNA microarray. Details of this expression profile are presented in Supplementary Table S2. We identified upregulation of many genes, and particularly noticed upregulation in the expression of genes encoding *ALDH1A1* and *ABC transporters*, which were

Table 1. EGFR-TKI–resistant cell lines and resistant mechanisms

Cell Line	Gefitinib exposure	Gefitinib IC_{50}, μmol/L	Erlotinib IC_{50}, μmol/L	*EGFR* T790M	*MET* amp	Other
HCC827	—	0.0076	0.0042	No	No	N/A
HCC827-GR-step	Stepwise	9.23	>10	No	Yes	—
HCC827-GR-high1	High	8.84	>10	No	No	EMT, stem cell–like properties
HCC827-GR-high2	High	>10	>10	No	No	EMT, stem cell–like properties *EGFR*-WT
PC-9	—	0.071	0.15	No	No	N/A
PC-9-GR-step	Stepwise	>10	>10	Yes	No	—
PC-9-GR-high	High	>10	>10	No	No	Unknown
HCC4006	—	0.024	0.034	No	No	N/A
HCC4006-GR-step	Stepwise	9.33	>10	No	No	EMT
HCC4006-GR-high	High	>10	>10	No	No	EMT
HCC4011	—	0.033	0.11	No	No	N/A
HCC4011-GR-step	Stepwise	5.07	>10	No	Yes	—
HCC4011-GR-high	High	6.48	>10	No	Yes	—

Abbreviations: amp, amplification; N/A, not applicable; WT, wild-type.

Published OnlineFirst March 29, 2013; DOI: 10.1158/0008-5472.CAN-12-4136

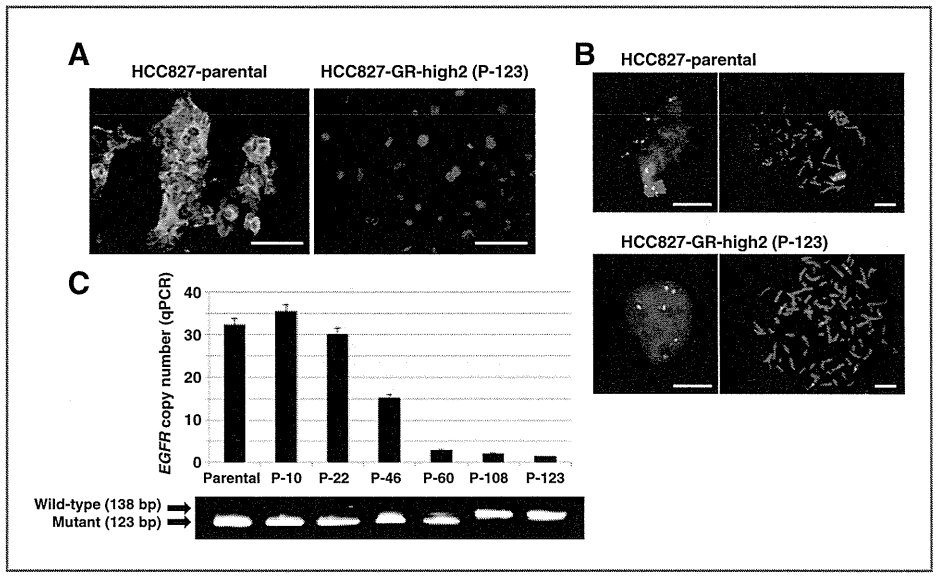

Figure 1. Loss of *EGFR*-mutant allele and progressive decrease of *EGFR* copy number in HCC827-derived resistant subline. HCC827-GR-high2 showed progressive decrease in the *EGFR*-mutant allele through the course of passages, leading to the disappearance of focally amplified *EGFR* alleles. A and B, fluorescence immunocytochemistry of *EGFR* E746-A750 deletion mutation-specific protein (A; green, mutation-specific protein; blue, nucleus) and FISH (B; red, *EGFR*; green, CEP7; blue, nucleus). C, progressive decrease in the *EGFR*-mutant allele by qPCR and PCR-based length polymorphism assay. P-, passage. Scale bars, 100 μm (A); 10 μm (B).

observed in the cells with stem cell–like properties. The upregulation of stem cell-related markers such as *ALDH1A1*, *ABC transporters*, and *CD44* was confirmed by qRT-PCR (Fig. 2). In addition, the upregulation of *ALDH1A1* in HCC827-GR-highs was confirmed by Western blotting and fluorescent immunocytochemistry (Supplementary Fig. S2C and S2D). *ALDH1A1* was not detected in the other sublines.

We conducted phospho-RTK array and phospho-kinase array to find no significant differences including AXL between parental HCC827 and HCC827-GR-highs, except for the downregulation of phosphorylated EGFR protein in HCC827-GR-highs (Supplementary Fig. S3).

Expression status of miR-200 family in resistant cell lines with EMT features

The result of cDNA microarray in HCC827-GR-high2 indicated the upregulation of Zinc-finger enhancer binding (ZEB) transcription factors (ZEB1 and ZEB2), which are crucial EMT activators (25–27). Because EMT was reported to be regulated by miR-200 family targeting *ZEB1* and *ZEB2*, we analyzed the expression status of the miR-200 family by qRT-PCR. As shown in Fig. 3A, miR-200a, miR-200b, and miR-200c were downregulated in both HCC827- and HCC4006-derived resistant sublines with EMT features. In particular, miR-200c was extensively downregulated in HCC827-GR-highs compared with parental HCC827. To investigate the mechanism of downregulation of miR-200 family, we examined the methylation status of miR-200 family by MSP (Fig. 3B) and bisulfite genomic sequencing (data not shown). Our results indicate that miR-200 families were methylated and their expressions were recovered following treatment with 5-aza-2′-deoxycytidine (Fig. 3C).

Stem cell–like property in acquiring resistance

Upregulation of ALDH1A1 and ABC transporters suggests that HCC827-GR-highs may acquire stem cell–like properties. Thus, we quantified the side population by dual wavelength flow cytometry. We found an extreme increase in the number of side-population cells in HCC827-GR-highs as illustrated in Fig. 4A. The majority of the side-population fraction in HCC827-GR-highs was eliminated in the presence of verapamil, indicating the specificity of the side population. In addition, we conducted a sphere formation assay to examine the cellular functional features of stem cell–like properties. We found that HCC827-GR-highs acquired higher ability to form spheres in suspension culture compared with parental HCC827 and HCC827-GR-step (Fig. 4B). To examine the stem cell–like properties *in vivo*, we conducted tumor transplantation experiments (28, 29). We subcutaneously implanted HCC827, HCC827-GR-high1, and HCC827-GR-high2 cells to examine the tumor-forming capability in NOD/SCID mice. We found that HCC827-GR-highs exhibited higher tumorigenicity than parental HCC827 cells did. The HCC827-GR-highs established larger tumors with shorter latencies than the parental HCC827 cells did (Fig. 4C). HCC827-GR-highs showed a significant increase in the expression of ALDH1A1, as indicated by IHC staining (Supplementary Fig. S4). These results further indicate that HCC827-GR-highs acquired stem cell–like properties. Of interest, the histologic finding of HCC827-GR-highs was different from that of parental HCC827 (Supplementary Fig. S4). Even after culturing of HCC827-GR-highs with gefitinib-free medium for 6 months, HCC827-GR-high2 still exhibited both the EMT and stem cell–like features, and did not exhibit production of *EGFR*-mutant–specific protein or further increase of either mutant allele or *EGFR* copy number (Supplementary Fig. S5). The appearance of stem cell–like properties in HCC827-resistant sublines established by high-concentration method was independently confirmed in 3 additional different culture dishes.

Gefitinib sensitivity of HCC827 and HCC827-GR-high2 hybridoma

A hybridoma model was generated with parental and resistant cells to distinguish whether the causative factor for

Published OnlineFirst March 29, 2013; DOI: 10.1158/0008-5472.CAN-12-4136

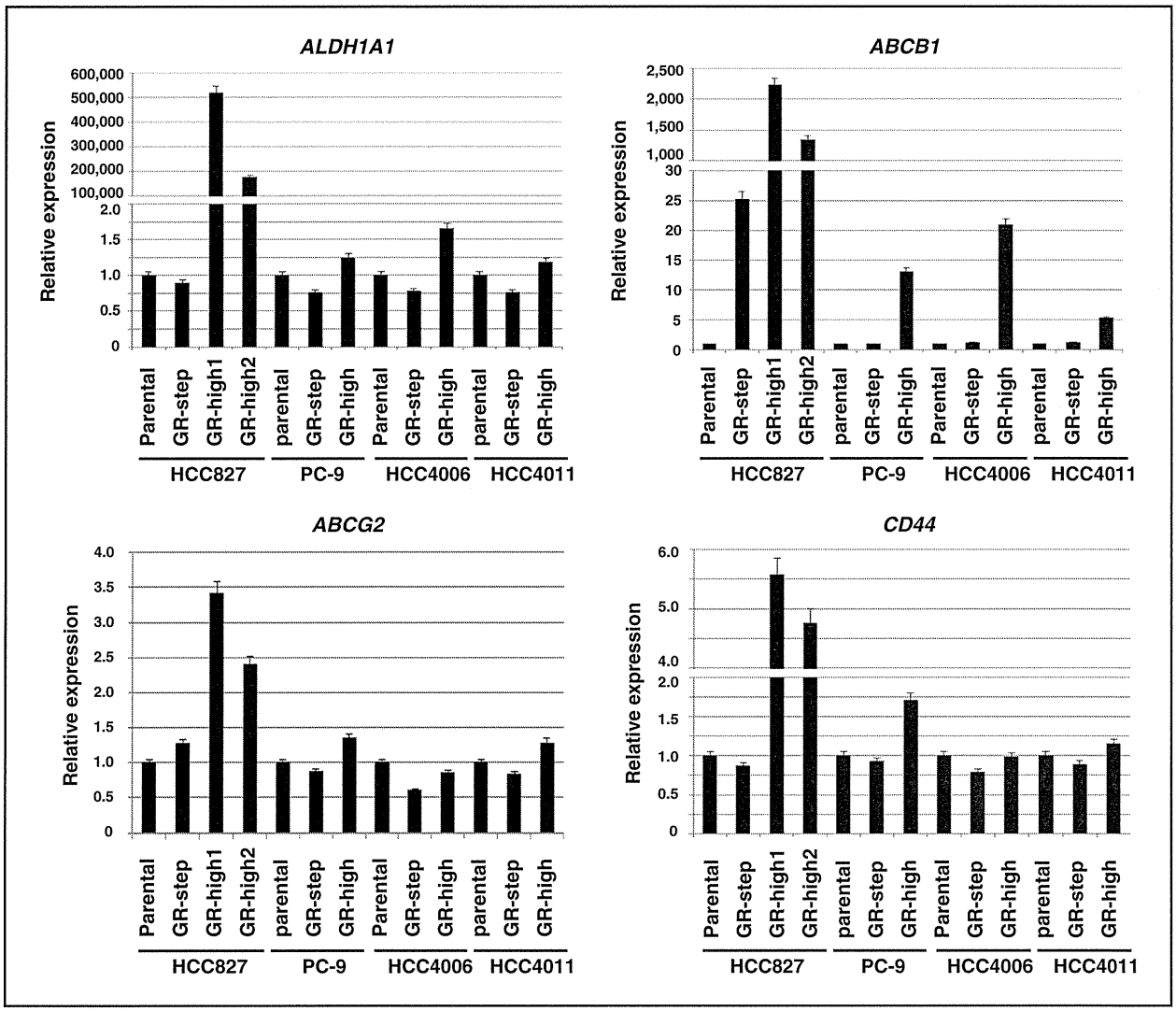

Figure 2. Relative gene expression levels of stem cell–related markers by qRT-PCR. The mRNA expressions of *ALDH1A1*, *ABCB1*, *ABCG2*, and *CD44* were confirmed by qRT-PCR. The expression of stem cell–related markers *ALDH1A1*, *ABCG2*, and *CD44* were higher than that of the parental line in HCC827-GR-highs. In addition, the expression of *ABCB1* was significantly higher than that of the parental line in HCC827-GR-step, HCC827-GR-highs, PC-9-GR-high, and HCC4006-GR-high.

EGFR-TKI resistance in HCC827-GR-high2 that exhibited loss of mutant *EGFR* alleles, EMT, and stem cell–like properties involved either loss- or gain-of-function. A hybridoma cell line was generated by fusing HCC827 with HCC827-GR-high2, which was then treated with gefitinib. The hybridoma exhibited resistance to gefitinib at a concentration of 2 μmol/L, indicating that the resistant cells had acquired drug-resistant properties to parental cells, rather than having lost drug sensitivity.

Sensitivity to various drugs in each cell line

Drug sensitivities against various agents are shown in Table 2. The sublines of HCC827, PC-9, and HCC4006 generated under high concentrations of gefitinib exhibited higher IC_{50} values for docetaxel and paclitaxel than those of parental cells. Moreover, we examined the antitumor effects of histone deacetylase (HDAC) inhibitors [trichostatin A and vorinostat (SAHA)] and a proteasome inhibitor (bortezomib). These inhibitors produced moderate to strong antitumor effects in both parental and resistant cells, which did not acquire resistance to these drugs (Table 2; refs. 30, 31).

Molecular profile of EGFR-TKI–resistant clinical samples

Clinical tumor samples, which showed acquired resistance to TKIs, were collected both before and after TKI treatment and examined genetically and immunohistologically (Table 3). Among 16 cases with acquired resistance to TKIs, corresponding pretreatment samples were available in 3 cases (no. 1, 5, and 16). After acquiring resistance, 3 cases exhibited *EGFR* T790M

Published OnlineFirst March 29, 2013; DOI: 10.1158/0008-5472.CAN-12-4136

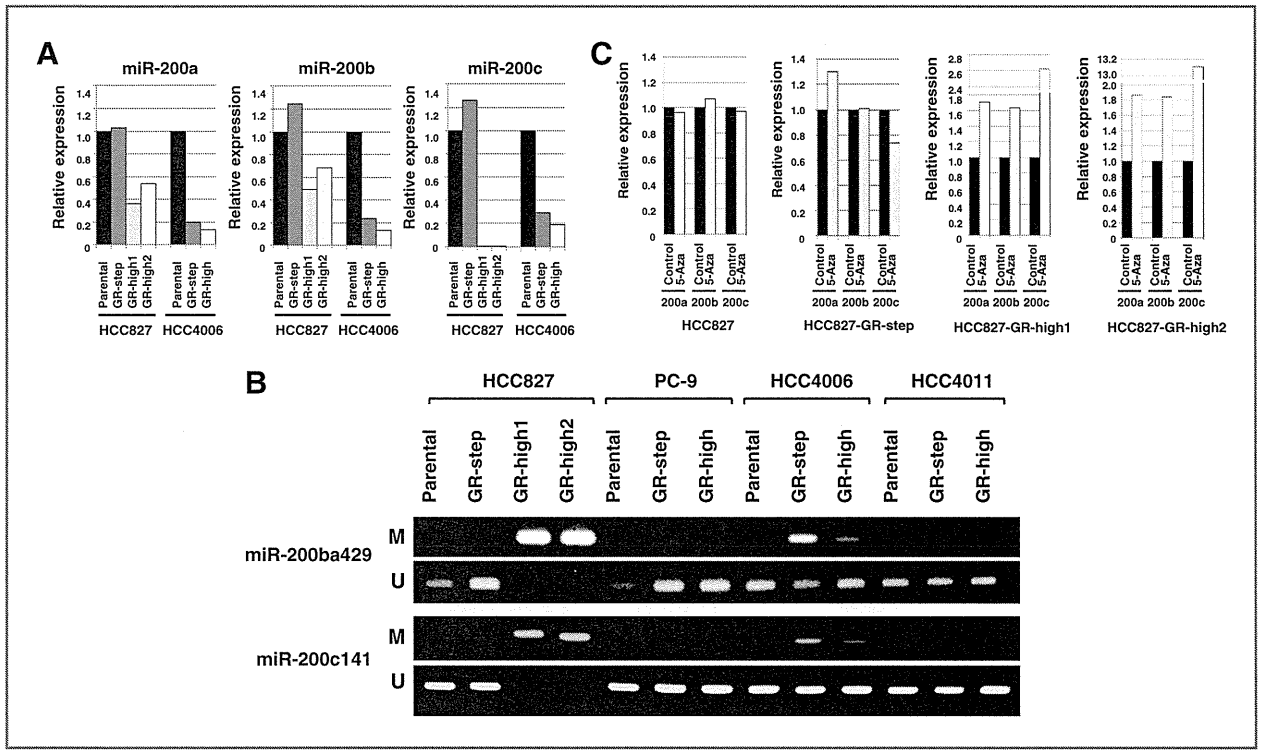

Figure 3. CpG island hypermethylation-associated silencing of the miR-200 family in acquired resistance to EGFR-TKI sublines with EMT features. A, the expression of miR-200 family was extensively downregulated in resistant sublines with EMT features compared with parental lines by qRT-PCR. B, the MSP revealed the hypermethylation of miR-200 family in resistant cells with EMT features. C, the miR-200 family expressions were recovered following treatment with DNA-demethylating agent 5-aza-2′-deoxycytidine (5-Aza) in miR-200 family methylated cells. M, methylated; U, unmethylated.

mutation and 2 exhibited *MET* amplification. In addition, some samples harboring EMT features (based on E-cadherin and vimentin expression status) also exhibited expression of stem cell–related markers ALDH1A1 and ABCB1, determined by IHC staining (Fig. 4D). In total, 5 of 16 cases exhibited ALDH1A1 expression in samples that showed acquired resistance to TKI. In 3 cases whose pretreatment samples were available, ALDH1A1 was not expressed prior to TKI treatment. Among them, 2 cases (no. 5 and 16) exhibited ALDH1A1 expression after acquiring resistance to TKI. Of note, case no. 5 was a patient with recurrent lung cancer after surgery and no other anticancer drugs except gefitinib and erlotinib were administrated.

Discussion

In this study, we showed that the method of drug exposure in cell culture influences the mechanisms of acquired resistance to EGFR-TKI. Studies using *EGFR*-mutant cell lines have indicated that the different types of resistance mechanisms are determined within the individual cell lines in response to certain conditions. For instance, both PC-9 and H3255 are known to develop resistance to EGFR-TKIs through *EGFR* T790M mutation as a result of stepwise escalation exposure (22, 23). On the other hand, HCC827 is known to overcome EGFR-TKI through *MET* amplification (8, 32). Interestingly, Suda and colleagues reported that HCC827 cells developed the T790M mutation under the inhibition of MET signaling, suggesting that the microenvironment of the tumor cells influenced the mechanisms of resistance (32). Indeed, in an analysis using multiple gefitinib refractory tumors obtained from autopsies, the lesions from patients exhibited T790M and/or *MET* amplification depending on the lesion sites (32). In addition to these resistance mechanisms accompanying somatic gene alterations, recent studies have indicated that some biologic signatures such as acquisition of EMT phenotype and transformation to SCLC were associated with EGFR-TKI resistance, the causative genetic alterations of which are not known (11, 33, 34). EMT was observed in HCC4006 sublines and HCC827-GR-highs, but not in HCC827-GR-step sublines. Summarily, these observations suggest that cancer cells might be able to enact different mechanisms based on the microenvironment to survive and escape cell death from apoptotic pressure of EGFR-TKI.

Among identified EMT-related genes, *ZEB1* expression was reported to be most significantly correlated with mesenchymal phenotype in human malignancies including NSCLC (25, 26). The cDNA array revealed upregulation of *ZEB1* and *ZEB2* expression in HCC827-GR-high2 and we consequently focused on the miR-200 family, which is reported to repress *ZEB1* as a key regulator of EMT (35). Indeed, our results indicate downregulated expression of the miR-200 family, especially miR-200c, in resistant sublines with EMT features. Moreover, a recent study has indicated that loss of miR-200c expression with DNA methylation is associated with chemoresistant

Published OnlineFirst March 29, 2013; DOI: 10.1158/0008-5472.CAN-12-4136

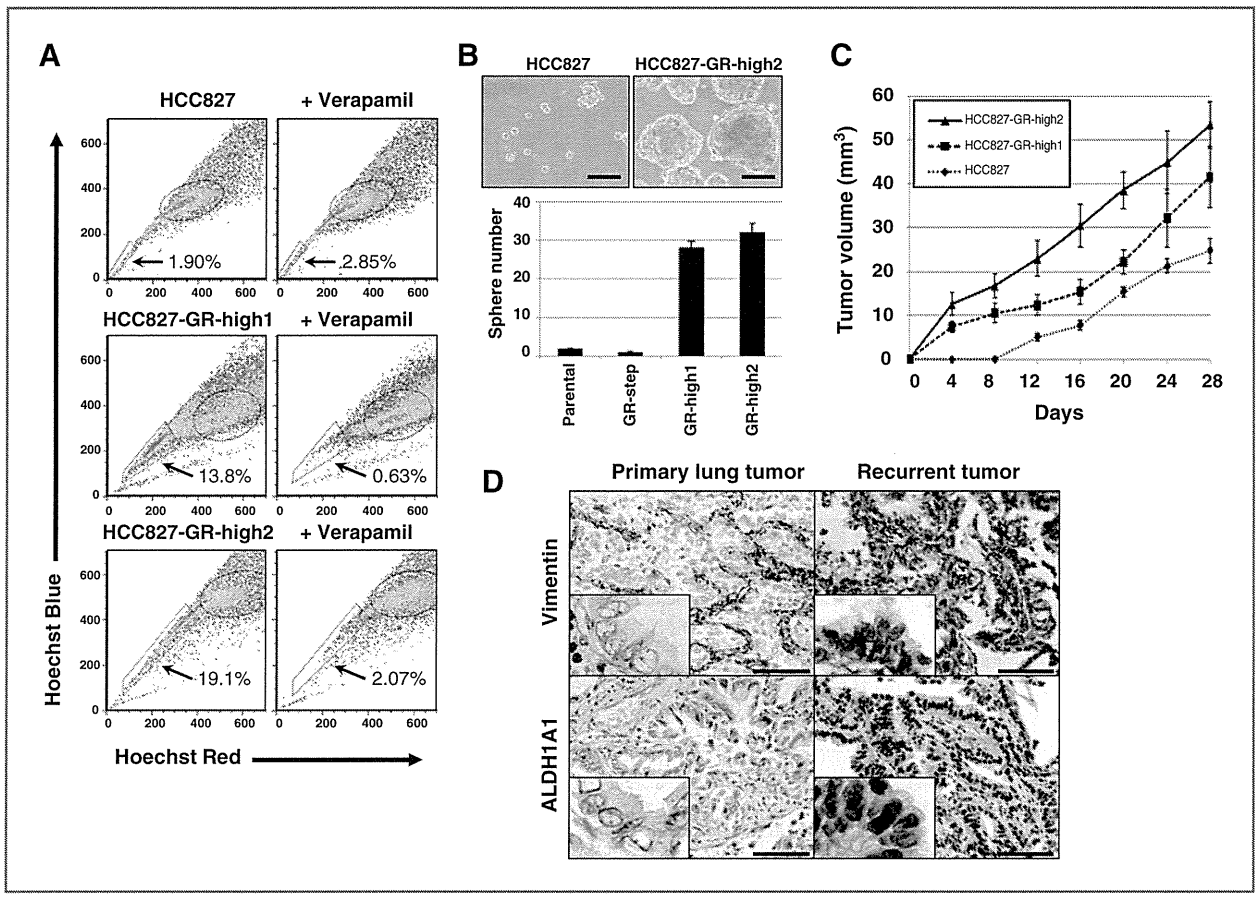

Figure 4. Emergence of the stem cell–like properties in acquiring resistance to EGFR-TKI cells. A, side population analysis shows the extreme increase of side-population cells in HCC827-GR-highs compared with parental cells. The majority of the side-population fraction in HCC827-GR-highs was eliminated in the presence of verapamil. B, by sphere formation assay, HCC827-GR-highs acquired high ability to form spheres in suspension culture. C, the HCC827-GR-highs established larger tumors with shorter latencies than the parental HCC827 cells did in NOD/SCID mice, indicating HCC827-GR-highs exhibited higher tumorigenicity than parental HCC827 cells. D, representative images of IHC staining of pretreatment and recurrent tumor after EGFR-TKI treatment (case no. 5). The postresistant biopsy (right) shows an EMT feature with positive IHC staining for vimentin with expression of stem cell–related marker ALDH1A1. Scale bars, 100 μm.

phenotype in NSCLC (36). Of note, it is now known that EMT activators not only activate cellular motility but are also associated with the maintenance of stem cell properties and cell survival (37, 38). Our findings present the novel insight that the repression of miR-200 family by DNA methylation is responsible for EMT during the acquisition of resistance to EGFR-TKI.

As an important finding, some resistant cells with EMT signatures exhibited stem cell–like properties. Cancer stem cells (CSC), which are characterized by the capacity for pluripotency and self-renewal, have been attracting interest as a source of cancer cells (39). The significance of stem cell–like properties in lung cancer has been investigated in both basic and clinical research (40, 41). However, the CSC of lung cancers remains a subject of ongoing research, and its specific makers have not yet been identified. In our study, several cell surface proteins, including CD133, that may be candidate markers of general CSC, were not upregulated in resistant sublines. These results collectively suggest that understanding and overcoming drug resistance from the viewpoint of stem cell identity may present new and challenging opportunities.

We examined the sensitivity of various types of drugs, including conventional chemotherapeutic agents, HDAC inhibitors, and proteasome inhibitor, to resistant sublines. HCC827-GR-highs, HCC4006-GR-high, and PC-9-GR-high exhibited significant resistance to docetaxel and paclitaxel, but not to cisplatin. This result is reasonable because docetaxel and paclitaxel, unlike cisplatin, are considered to be effluxed by the ABC transporter system, which was upregulated in these sublines. These results would lead to selection of appropriate chemotherapeutic drugs following acquired resistance to EGFR-TKI.

In our study, clinically usable HDAC inhibitor and proteasome inhibitor SAHA and bortezomib exhibited similar antitumor efficacy for both parental and resistant cells. Clinical studies have shown that SAHA is effective for NSCLC when combined with other cancer therapies (42, 43). Notably, HDAC inhibitors are reported to be effective in treating chronic

Published OnlineFirst March 29, 2013; DOI: 10.1158/0008-5472.CAN-12-4136

Table 2. IC_{50} values (μmol/L) against various agents

	Chemotherapeutic agent			HDAC inhibitor		Proteasome inhibitor
Cell line	CDDP	DOC	PTX	TSA	SAHA	Bortezomib
HCC827	4.51	0.0021	0.0032	0.082	1.85	0.0044
HCC827-GR-step	4.29	0.0020	0.0020	0.092	0.63	0.0072
HCC827-GR-high1	4.45	0.022[a]	0.15[a]	0.097	2.05	0.0061
HCC827-GR-high2	8.04	0.51[a]	1.46[a]	0.092	2.20	0.0074
PC-9	2.92	0.00066	0.0014	0.020	1.06	0.0097
PC-9-GR-step	2.49	0.0060	0.0014	0.018	1.14	0.0073
PC-9-GR-high	5.64	0.0020[a]	0.0022	0.026	1.03	0.017
HCC4006	>10	0.038	0.038	0.55	9.15	0.13
HCC4006-GR-step	>10	0.025	0.015	0.13	5.94	0.14
HCC4006-GR-high	>10	0.824[a]	1.10[a]	2.22	8.20	0.15
HCC4011	>10	0.0011	0.0014	0.021	0.97	0.0033
HCC4011-GR-step	>10	0.00069	0.0017	0.017	0.86	0.0061
HCC4011-GR-high	>10	0.00034	0.0014	0.018	0.93	0.0055

Abbreviations: CDDP, cisplatin; DOC, docetaxel; PTX, paclitaxel; TSA, trichostatin A.
[a]The ratio of the IC_{50} value in each resistant line to the parental line is higher than 10 times.

myelogenous leukemia, in which stem cells appeared after the acquisition of resistance to imatinib mesylate (44). The proteasome inhibitor, bortezomib failed to produce antitumor effects either alone or in conjunction with other drugs in a clinical trial, although preliminary data suggested that bortezomib as a single agent may show antitumor activity in patients with NSCLC (45, 46). However, current research is rapidly working toward the development of next-generation proteasome inhibitors (47), and our data indicating that bortezomib activity was not influenced by the EGFR-TKI resistance state may be useful for the future development of proteasome inhibitors.

Our results support the usefulness of *in vitro* experiment to investigate the mechanisms of resistance to EGFR-TKI. In the pharmacokinetic analysis of gefitinib, the plasma concentration of gefitinib was found to reach a steady-state level within 7 days, in most of the cases (48). Nakamura and colleagues

Table 3. Acquired resistance to EGFR-TKIs; clinical samples

					Immunohistochemistry		
No.	Age	Sex	*EGFR* mutation	Genetic alteration	Vimentin	ALDH1A1	ABCB1
1	88	F	L858R	T790M	−/−	−/−	+/+
2	72	F	19 del	T790M	N/A	N/A	N/A
3	53	F	19 del		N/A	N/A	N/A
4	34	F	19 del	Loss of *EGFR*-mut	+	N/A	N/A
5	75	F	L858R		−/+	−/+	+/+
6	43	M	19 del		−	−	+
7	73	F	19 del	*MET* amp	−	−	+
8	62	F	19 del		+	−	−
9	70	M	19 del	*MET* amp	−	−	+
10	52	F	19 del	T790M	−	−	+
11	49	M	L858R		+	+	+
12	65	M	L858R		−	−	+
13	43	M	19 del		−	−	+
14	59	F	G719C		−	+	+
15	53	M	L858R		+	+	+
16	71	F	L858R		−/+	−/+	+/+

NOTE: Among 16 cases with acquired resistance to TKIs, corresponding pretreatment samples were available in 3 cases (no. 1, 5, and 16).
Abbreviations: amp, amplification; del, deletion; mut, mutation; N/A, not applicable.

Published OnlineFirst March 29, 2013; DOI: 10.1158/0008-5472.CAN-12-4136

reported that the plasma concentration of gefitinib in patients receiving 250 mg gefitinib daily ranged from 115 to 2,012 ng/mL (0.257–4.502 μmol/L) on day 3 (D3) and 126 to 2,926 ng/mL (0.282–6.547 μmol/L) on day 8 (D8), whereas the median D8-to-D3 ratio was 1.578 and ranged from 0.758 to 6.094 (49). These results indicate considerable variation in plasma concentration and the pharmacokinetics of gefitinib according to individual patients. Of note, D8-to-D3 ratio under 1.0 indicates that drug concentration may reach a plateau shortly after initiation of gefitinib treatment. This condition may be similar to that of drug contact to cells in our high-concentration method. In addition, Haura and colleagues reported that tumor levels during treatment with gefitinib were higher than, but not related to, plasma levels (50). Further resistance-related research will require additional elaboration about culture conditions and microenvironment.

It is still not known what caused the emergence of stem cell–like properties in HCC827-GR-highs; however, 2 possibilities should be considered: (i) high-concentration exposure induces cells with stem cell–like properties; and (ii) the cells with stem cell–like properties existed as minor clones in HCC827 prior to gefitinib exposure, and these were finally selected as the major clones. For the latter possibility, it is also not clear as to why cells with stem-like properties appeared as the major population only from the high-concentration exposure method.

In conclusion, culture conditions with EGFR-TKI seem to influence the mechanism of acquired resistance, suggesting that the microenvironment is a determinating factor for the mechanisms underlying acquisition of resistance to EGFR-TKI. Our study indicated that EGFR-TKI treatment induced stem cell–like properties and is associated with EGFR-TKI resistance.

Disclosure of Potential Conflicts of Interest

No potential conflicts of interest were disclosed.

Authors' Contributions

Conception and design: K. Shien, S. Toyooka, Y. Maki, A.F. Gazdar
Development of methodology: K. Shien, S. Toyooka, H. Asano
Acquisition of data (provided animals, acquired and managed patients, provided facilities, etc.): K. Shien, S. Toyooka, S. Hashida, N. Takigawa, K. Kiura, S. Miyoshi
Analysis and interpretation of data (e.g., statistical analysis, biostatistics, computational analysis): K. Shien, J. Soh, K.L. Thu, W.L. Lam
Writing, review, and/or revision of the manuscript: K. Shien, S. Toyooka, H. Yamamoto, J. Soh, E. Ichihara, A.F. Gazdar, W.L. Lam, S. Miyoshi
Administrative, technical, or material support (i.e., reporting or organizing data, constructing databases): K. Shien, S. Toyooka, M. Jida, Y. Maki
Study supervision: H. Asano, K. Tsukuda, S. Miyoshi

Acknowledgments

The authors thank Ms. Fumiko Isobe (Department of Cancer and Thoracic Surgery, Okayama University Graduate School of Medicine, Dentistry and Pharmaceutical Sciences, Okayama, Japan) for her excellent technical support.

The costs of publication of this article were defrayed in part by the payment of page charges. This article must therefore be hereby marked *advertisement* in accordance with 18 U.S.C. Section 1734 solely to indicate this fact.

Received November 9, 2012; revised February 8, 2013; accepted February 19, 2013; published OnlineFirst March 29, 2013.

References

1. Lynch TJ, Bell DW, Sordella R, Gurubhagavatula S, Okimoto RA, Brannigan BW, et al. Activating mutations in the epidermal growth factor receptor underlying responsiveness of non–small-cell lung cancer to gefitinib. N Engl J Med 2004;350:2129–39.
2. Paez JG, Jänne PA, Lee JC, Tracy S, Greulich H, Gabriel S, et al. EGFR mutations in lung cancer: correlation with clinical response to gefitinib therapy. Science 2004;304:1497–500.
3. Mok TS, Wu YL, Thongprasert S, Yang CH, Chu DT, Saijo N, et al. Gefitinib or carboplatin–paclitaxel in pulmonary adenocarcinoma. N Engl J Med 2009;361:947–57.
4. Maemondo M, Inoue A, Kobayashi K, Sugawara S, Oizumi S, Isobe H, et al. Gefitinib or chemotherapy for non–small-cell lung cancer with mutated EGFR. N Engl J Med 2010;362:2380–8.
5. Mitsudomi T, Morita S, Yatabe Y, Negoro S, Okamoto I, Tsurutani J, et al. Gefitinib versus cisplatin plus docetaxel in patients with non–small-cell lung cancer harbouring mutations of the epidermal growth factor receptor (WJTOG3405): an open label, randomised phase 3 trial. Lancet Oncol 2010;11:121–8.
6. Kobayashi S, Boggon TJ, Dayaram T, Jänne PA, Kocher O, Meyerson M, et al. EGFR mutation and resistance of non–small-cell lung cancer to gefitinib. N Engl J Med 2005;352:786–92.
7. Pao W, Miller VA, Politi KA, Riely GJ, Somwar R, Zakowski MF, et al. Acquired resistance of lung adenocarcinomas to gefitinib or erlotinib is associated with a second mutation in the EGFR kinase domain. PLoS Med 2005;2:e73.
8. Engelman JA, Zejnullahu K, Mitsudomi T, Song Y, Hyland C, Park JO, et al. MET amplification leads to gefitinib resistance in lung cancer by activating ERBB3 signaling. Science 2007;316:1039–43.
9. Bean J, Brennan C, Shih JY, Riely G, Viale A, Wang L, et al. MET amplification occurs with or without T790M mutations in EGFR mutant lung tumors with acquired resistance to gefitinib or erlotinib. Proc Natl Acad Sci U S A 2007;104:20932–7.
10. Yano S, Wang W, Li Q, Matsumoto K, Sakurama H, Nakamura T, et al. Hepatocyte growth factor induces gefitinib resistance of lung adenocarcinoma with epidermal growth factor receptor-activating mutations. Cancer Res 2008;68:9479–87.
11. Sequist LV, Waltman BA, Dias-Santagata D, Digumarthy S, Turke AB, Fidias P, et al. Genotypic and histological evolution of lung cancers acquiring resistance to EGFR inhibitors. Sci Transl Med 2011;3:75ra26.
12. Zhang Z, Lee JC, Lin L, Olivas V, Au V, Laframboise T, et al. Activation of the AXL kinase causes resistance to EGFR-targeted therapy in lung cancer. Nat Genet 2012;44:852–60.
13. Tabara K, Kanda R, Sonoda K, Kubo T, Murakami Y, Kawahara A, et al. Loss of activating EGFR mutant gene contributes to acquired resistance to EGFR tyrosine kinase inhibitors in lung cancer cells. PLoS ONE 2012;7:e41017.
14. Sagawa Y, Fujitoh A, Nishi H, Ito H, Yudate T, Isaka K. Establishment of three cisplatin-resistant endometrial cancer cell lines using two methods of cisplatin exposure. Tumour Biol 2011;32:399–408.
15. Shien K, Ueno T, Tsukuda K, Soh J, Suda K, Kubo T, et al. Knockdown of the epidermal growth factor receptor gene to investigate its therapeutic potential for the treatment of non–small-cell lung cancers. Clin Lung Cancer 2012;13:488–93.
16. Asano H, Toyooka S, Tokumo M, Ichimura K, Aoe K, Ito S, et al. Detection of EGFR gene mutation in lung cancer by mutant-enriched polymerase chain reaction assay. Clin Cancer Res 2006;12:43–8.
17. Soh J, Okumura N, Lockwood WW, Yamamoto H, Shigematsu H, Zhang W, et al. Oncogene mutations, copy number gains and mutant allele specific imbalance (MASI) frequently occur together in tumor cells. PLoS ONE 2009;4:e7464.
18. Kubo T, Yamamoto H, Lockwood WW, Valencia I, Soh J, Peyton M, et al. MET gene amplification or EGFR mutation activate MET in lung

Published OnlineFirst March 29, 2013; DOI: 10.1158/0008-5472.CAN-12-4136

cancers untreated with EGFR tyrosine kinase inhibitors. Int J Cancer 2009;124:1778–84.
19. Davalos V, Moutinho C, Villanueva A, Boque R, Silva P, Carneiro F, et al. Dynamic epigenetic regulation of the microRNA-200 family mediates epithelial and mesenchymal transitions in human tumorigenesis. Oncogene 2012;31:2062–74.
20. Goodell MA, Brose K, Paradis G, Conner AS, Mulligan RC. Isolation and functional properties of murine hematopoietic stem cells that are replicating *in vivo*. J Exp Med 1996;183:1797–806.
21. Shien K, Toyooka S, Ichimura K, Soh J, Furukawa M, Maki Y, et al. Prognostic impact of cancer stem cell-related markers in non–small cell lung cancer patients treated with induction chemoradiotherapy. Lung Cancer 2012;77:162–7.
22. Ogino A, Kitao H, Hirano S, Uchida A, Ishiai M, Kozuki T, et al. Emergence of epidermal growth factor receptor T790M mutation during chronic exposure to gefitinib in a non small cell lung cancer cell line. Cancer Res 2007;67:7807–14.
23. Engelman JA, Mukohara T, Zejnullahu K, Lifshits E, Borrás AM, Gale CM, et al. Allelic dilution obscures detection of a biologically significant resistance mutation in EGFR-amplified lung cancer. J Clin Invest 2006;116:2695–706.
24. Ohashi K, Sequist LV, Arcila ME, Moran T, Chmielecki J, Lin YL, et al. Lung cancers with acquired resistance to EGFR inhibitors occasionally harbor BRAF gene mutations but lack mutations in KRAS, NRAS, or MEK1. Proc Natl Acad Sci U S A 2012;109:E2127–33.
25. Gregory PA, Bert AG, Paterson EL, Barry SC, Tsykin A, Farshid G, et al. The miR-200 family and miR-205 regulate epithelial to mesenchymal transition by targeting ZEB1 and SIP1. Nat Cell Biol 2008;10:593–601.
26. Park SM, Gaur AB, Lengyel E, Peter ME. The miR-200 family determines the epithelial phenotype of cancer cells by targeting the E-cadherin repressors ZEB1 and ZEB2. Genes Dev 2008;22:894–907.
27. Brabletz S, Brabletz T. The ZEB/miR-200 feedback loop–a motor of cellular plasticity in development and cancer? EMBO Rep 2010;11: 670–7.
28. Visvader JE, Lindeman GJ. Cancer stem cells in solid tumours: accumulating evidence and unresolved questions. Nat Rev Cancer 2008;8: 755–68.
29. Rosen JM, Jordan CT. The increasing complexity of the cancer stem cell paradigm. Science 2009;324:1670–3.
30. Miyanaga A, Gemma A, Noro R, Kataoka K, Matsuda K, Nara M, et al. Antitumor activity of histone deacetylase inhibitors in non–small cell lung cancer cells: development of a molecular predictive model. Mol Cancer Ther 2008;7:1923–30.
31. Scagliotti G. Proteasome inhibitors in lung cancer. Crit Rev Oncol Hematol 2006;58:177–89.
32. Suda K, Murakami I, Katayama T, Tomizawa K, Osada H, Sekido Y, et al. Reciprocal and complementary role of MET amplification and EGFR T790M mutation in acquired resistance to kinase inhibitors in lung cancer. Clin Cancer Res 2010;16:5489–98.
33. Rho JK, Choi YJ, Lee JK, Ryoo BY, Na II, Yang SH, et al. Epithelial to mesenchymal transition derived from repeated exposure to gefitinib determines the sensitivity to EGFR inhibitors in A549, a non–small cell lung cancer cell line. Lung Cancer 2009;63:219–26.
34. Suda K, Tomizawa K, Fujii M, Murakami H, Osada H, Maehara Y, et al. Epithelial to mesenchymal transition in an epidermal growth factor receptor-mutant lung cancer cell line with acquired resistance to erlotinib. J Thorac Oncol 2011;6:1152–61.
35. Mongroo PS, Rustgi AK. The role of the miR-200 family in epithelial–mesenchymal transition. Cancer Biol Ther 2010;10:219–22.
36. Ceppi P, Mudduluru G, Kumarswamy R, Rapa I, Scagliotti GV, Papotti M, et al. Loss of miR-200c expression induces an aggressive, invasive, and chemoresistant phenotype in non–small cell lung cancer. Mol Cancer Res 2010;8:1207–16.
37. Mani SA, Guo W, Liao MJ, Eaton EN, Ayyanan A, Zhou AY, et al. The epithelial–mesenchymal transition generates cells with properties of stem cells. Cell 2008;133:704–15.
38. Morel AP, Lièvre M, Thomas C, Hinkal G, Ansieau S, Puisieux A. Generation of breast cancer stem cells through epithelial–mesenchymal transition. PLoS ONE 2008;3:e2888.
39. Reya T, Morrison SJ, Clarke MF, Weissman IL. Stem cells, cancer, and cancer stem cells. Nature 2001;414:105–11.
40. Eramo A, Lotti F, Sette G, Pilozzi E, Biffoni M, Di Virgilio A, et al. Identification and expansion of the tumorigenic lung cancer stem cell population. Cell Death Differ 2008;15:504–14.
41. Berns A. Stem cells for lung cancer? Cell 2005;121:811–3.
42. Ramalingam SS, Maitland ML, Frankel P, Argiris AE, Koczywas M, Gitlitz B, et al. Carboplatin and Paclitaxel in combination with either vorinostat or placebo for first-line therapy of advanced non–small-cell lung cancer. J Clin Oncol 2010;28:56–62.
43. Traynor AM, Dubey S, Eickhoff JC, Kolesar JM, Schell K, Huie MS, et al. Vorinostat (NSC# 701852) in patients with relapsed non–small cell lung cancer: a Wisconsin Oncology Network phase II study. J Thorac Oncol 2009;4:522–6.
44. Zhang B, Strauss AC, Chu S, Li M, Ho Y, Shiang KD, et al. Effective targeting of quiescent chronic myelogenous leukemia stem cells by histone deacetylase inhibitors in combination with imatinib mesylate. Cancer Cell 2010;17:427–42.
45. Fanucchi MP, Fossella FV, Belt R, Natale R, Fidias P, Carbone DP, et al. Randomized phase II study of bortezomib alone and bortezomib in combination with docetaxel in previously treated advanced non–small-cell lung cancer. J Clin Oncol 2006;24:5025–33.
46. Ramalingam SS, Davies AM, Longmate J, Edelman MJ, Lara PN Jr, Vokes EE, et al. Bortezomib for patients with advanced-stage bronchioloalveolar carcinoma: a California Cancer Consortium Phase II study (NCI 7003). J Thorac Oncol 2011;6:1741–5.
47. Dick LR, Fleming PE. Building on bortezomib: second-generation proteasome inhibitors as anti-cancer therapy. Drug Discov Today 2010;15:243–9.
48. Baselga J, Rischin D, Ranson M, Calvert H, Raymond E, Kieback DG, et al. Phase I safety, pharmacokinetic, and pharmacodynamic trial of ZD1839, a selective oral epidermal growth factor receptor tyrosine kinase inhibitor, in patients with five selected solid tumor types. J Clin Oncol 2002;20:4292–302.
49. Nakamura Y, Sano K, Soda H, Takatani H, Fukuda M, Nagashima S, et al. Pharmacokinetics of gefitinib predicts antitumor activity for advanced non–small cell lung cancer. J Thorac Oncol 2010;5:1404–9.
50. Haura EB, Sommers E, Song L, Chiappori A, Becker A. A pilot study of preoperative gefitinib for early-stage lung cancer to assess intratumor drug concentration and pathways mediating primary resistance. J Thorac Oncol 2010;5:1806–14.

Downregulation of microRNA-34 induces cell proliferation and invasion of human mesothelial cells

NORIMITSU TANAKA[1], SHINICHI TOYOOKA[1], JUNICHI SOH[1], KAZUNORI TSUKUDA[1], KAZUHIKO SHIEN[1], MASASHI FURUKAWA[1], TAKAYUKI MURAOKA[1], YUHO MAKI[1], TSUYOSHI UENO[1], HIROMASA YAMAMOTO[1], HIROAKI ASANO[1], TAKEMI OTSUKI[2] and SHINICHIRO MIYOSHI[1]

[1]Department of Thoracic Surgery, Okayama University Graduate School of Medicine, Dentistry and Pharmaceutical Sciences, Okayama 700-8558; [2]Department of Hygiene, Kawasaki Medical School, Kurashiki, Okayama 701-0192, Japan

Received October 24, 2012; Accepted December 14, 2012

DOI: 10.3892/or.2013.2351

Abstract. Malignant mesothelioma (MM) is an aggressive tumor with a dismal prognosis, and the molecular alterations involved in this disease remain unknown. We previously reported that microRNA-34s (miR-34s) are methylated and downregulated in MM and may play an important role in the carcinogenesis of MM. In this study, we downregulated miR-34s in human mesothelial cells to investigate the cellular effect of miR-34 knockdown. For the cell study, we used LP-9, a human mesothelial cell line, and three human primary-cultured mesothelial cell lines. RNA-based miR-34a, -34b and -34c inhibitors were transfected into these cells, and their effects on proliferation and invasion were evaluated. A scramble RNA oligonucleotide was used as a control. The protein expression status was estimated using western blotting. After miR-34 inhibitor transfection, miR-34a, -34b and -34c were downregulated in all the examined mesothelial cell lines. miR-34 inhibitor transfection significantly increased cell proliferation in all of the mesothelial cell lines, compared with the scramble control. The invasive ability also increased in the miR-34 inhibitor transfectants, compared with the scramble control, in the LP-9 cell line. Western blotting confirmed the upregulation of c-MET, phospho-c-MET, and Bcl-2 proteins in LP-9 cells after miR-34 inhibitor transfection. In conclusion, our study showed that the downregulation of miR-34s induced an oncogenic phenotype in non-malignant mesothelial cells. The present study, together with the results of our previous report, strongly suggest that miR-34s play an important role in the early carcinogenic process involved in the transformation of human mesothelial cells to MM.

Correspondence to: Dr Shinichi Toyooka, Department of General Thoracic Surgery, Okayama University Graduate School of Medicine, Dentistry and Pharmaceutical Sciences, 2-5-1 Shikata-cho, Kita-ku, Okayama 700-8558, Japan
E-mail: toyooka@md.okayama-u.ac.jp

Abbreviations: MM, malignant mesothelioma; miR, microRNA; HPMCs, human primary-cultured mesothelial cells

Key words: mesothelial cells, carcinogenesis, non-coding RNA, microRNA-34, mesothelioma

Introduction

Malignant mesothelioma (MM) is an aggressive tumor with a poor prognosis that arises most commonly in the pleura or peritoneum (1,2). MM was once a rare disease, but its incidence has increased worldwide, probably as a result of widespread exposure to asbestos (3). However, a standard curative modality, such as radiotherapy, conventional chemotherapy or molecular targeting therapy, has not yet been established for advanced MM. In addition, much less information regarding the molecular alterations involved in MM is available, compared with other solid neoplasms (4).

microRNAs (miRNAs) are a conserved class of non-coding 20-22 nt small RNAs that regulate protein expression by binding to mRNA, leading to mRNA degradation or the inhibition of translation (5-7). Among the miRNAs, the microRNA-34 (miR-34) family members are direct transcriptional targets of p53, constituting part of the p53 tumor-suppressive network and inducing cell cycle arrest, apoptosis and senescence, which are the major consequences of p53 activation (8,9). We previously reported that miR-34b/c was frequently downregulated by aberrant methylation in MM, resulting in the loss of tumor-suppressive p53 function and the acquisition of a malignant phenotype (10). One of the unique molecular features of MM is that mutations and deletions of the TP53 gene are rare (11), even though MM generally exhibits cell cycle alterations and anti-apoptosis, suggesting functional p53 deficiency (12).

In the present study, unlike our previous report, we downregulated miR-34s in human mesothelial cells to investigate the cellular biological effects of miR-34 inhibition in human mesothelial cells and to elucidate the cancer mechanisms involved in MM.

Materials and methods

Cell lines and cell culture. A human mesothelial cell line (LP-9, peritoneal mesothelial cells) and three types of human primary-cultured mesothelial cells (HPMCs) were used in

this study. The LP-9 cell line was purchased from the Coriell Cell Repository (Camden, NJ), and the three HPMCs were established from pleural effusions obtained from cancer-free patients treated at the Okayama University Hospital (Okayama, Japan), as described in our previous report (13). Approval from the Institutional Review Board and informed consent from all the patients were obtained.

LP-9 and HPMCs were cultured using Ham's F12 medium/Medium 199 (1:1 mixture) with 15% fetal bovine serum, 2 mM L-glutamine, 1.7 nM epidermal growth factor and 1100 nM hydrocortisone. All the cells were incubated at 37˚C in a humidified atmosphere with 5% CO_2.

Transfection of inhibitors of anti-miRNA-34s. LP-9 and the three HPMCs were transfected with a scramble control oligonucleotide or Anti-miR™ miR-34a, -34b and -34c inhibitors (Ambion, Austin, TX) after being seeded in 6-well plates. Each miRNA inhibitor (150 pmol) in 200 μl of serum-free antibiotic-free medium was mixed with 5 μl of Lipofectamine 2000 transfection reagent (Invitrogen, Carlsbad, CA) dissolved in 200 μl of the same medium and allowed to stand at room temperature for 20 min. The resulting 400 μl transfection solutions were then added to each well containing 1.6 ml of medium supplemented with 15% FBS. Cells were grown and harvested 48 h after the transfection for additional analyses.

Expression of miR-34s as determined using quantitative RT-PCR. The miRNA was isolated from LP-9 and mesothelial cells using the TaqMan MicroRNA Cells-to-CT™ kit (Ambion) and treated with DNase I (Ambion) to remove genomic DNA. A reverse transcriptional (RT) reaction was performed to extract 0.5 μg of miRNA using the TaqMan MicroRNA Reverse Transcriptional Kit system (Applied Biosystems) and TaqMan single RT primers for each miRNA (Applied Biosystems). Quantitative RT-PCR for miR-34a, -34b and -34c was performed using TaqMan MicroRNA Assay technology (Perkin-Elmer Corp., Foster City, CA) with the StepOnePlus™ Real-Time PCR system (Applied Biosystems). miR-374 expression was used to normalize the expression of the miR-34s as an endogenous control for the cell lines, following the manufacturer's recommendation (www.appliedbiosystems.com).

MTS assay. Cells were plated in 96-well plates at a density of $2.0x10^3$ cells/well. Cell viability was evaluated at 0 and 3 days using an MTS assay with CellTiter 96® AQueous One Solution reagent (Promega, Madison, WI).

Colony formation assay. The *in vitro* cell proliferation was assessed by liquid colony formation assay. Viable cells (100) were plated onto 6-well plates in triplicate. Cells were cultured and counted 14 days later after staining with 0.1% crystal violet in 20% ethanol for 5 min at room temperature. The number of visible colonies (>50 cells) was counted.

Immunohistochemistry for Ki-67. miR-34 inhibitor-transfected or scramble control-transfected LP-9 cells were grown and treated in Lab-Tek chamber slides (Nunc, Naperville, IL). Medium was aspirated and cells were fixed in 4% paraformaldehyde for 10 min at room temperature. Paraformaldehyde was aspirated, and the cells were treated with a 0.2% Tween 20 in PBS for 15 min. Cells were then washed in PBS, and Ki-67 (Novocastra, Newcastle, UK) was added at a dilution of 1:2,000 in 1% bovine serum albumin and incubation was carried out overnight at 4˚C. Cells were washed in PBS before incubating in the dark with an FITC-labeled secondary antibody (Jackson ImmunoResearch, West Grove, PA) at a dilution of 1:100 in 1% bovine serum albumin for 1 h. The secondary antibody solution was aspirated, and the cells were washed in PBS. Cells were incubated in the dark with 4',6-diamidino-2-phenylindole (1 μg/ml) in PBS for 30 min and washed, and coverslips were mounted with an anti-fade solution (Dako Corp., Carpinteria, CA). The Ki-67 staining was evaluated using labeling index. At least 1,000 cells were counted under a microscope at a magnification of x100.

Soft-agar colony formation assay. To investigate the anchorage-independent growth potential of miR-34 inhibition, we performed soft agar colony formation assay. Cells (7,500) in growth medium containing 0.4% agarose were placed on a 60-mm dish with a 0.5% agarose base. After 3 weeks of incubation, the colonies were stained with 0.005% crystal violet at room temperature for 1 h and were counted for each dish. A549 cells (human lung adenocarcinoma cell line) were used as a positive control.

Cell migration and invasion assays. Cell migration and invasion were assayed using a Boyden chamber assay with filter inserts (pore size, 8 μm) in 6-well dishes (BD Biosciences Discovery Labware, Bedford, MA). Tumor cells in 2 ml of serum-free medium (300 μl containing $0.75x10^5$ cells for the Transwell migration assay and $1.5x10^5$ cells for the Matrigel invasion assay) were added to the top chamber. The bottom chamber was prepared with 15% FBS as a chemoattractant. After a 24- and 48-h incubation for the migration and invasion assays, respectively, the non-invasive cells were removed by scrubbing with a cotton swab. The cells that migrated through the membrane and adhered to the lower surface of the membrane were fixed and stained using Diff-Quik stain (Sysmex, Kobe, Japan). To quantify the migration and invasion, the cells were counted under a microscope in 5 predetermined fields at a magnification of x100 and were represented as the average of three independent experiments.

Flow cytometric analysis. Cells were harvested and resuspended in PBS containing 0.2% Triton X-100 and 1 mg/ml RNase for 5 min at room temperature and then stained with propidium iodide (PI) at 50 mg/ml to determine subdiploid DNA content using a FACScan. Doublets, cell debris and fixation artifacts were gated out, and cell cycle analysis was carried out using CellQuest version 3.3 software.

Western blot analysis. Cells were grown to 80% confluence and harvested in lysis buffer [20 mmol/l Tris-HCl (pH 7.5), 150 mmol/l NaCl, 1 mmol/l Na_2EDTA, 1 mmol/l EGTA, 1% Triton, 2.5 mmol/l sodium pyrophosphate, 1 mmol/l β-glycerophosphate, 1 mmol/l Na_3VO_4, 1 μg/ml leupeptin] (Cell Signaling Technology, Beverly, MA) supplemented with Complete Mini (Roche, Basel, Switzerland) to extract the proteins. A total of 20 μg of protein was separated using

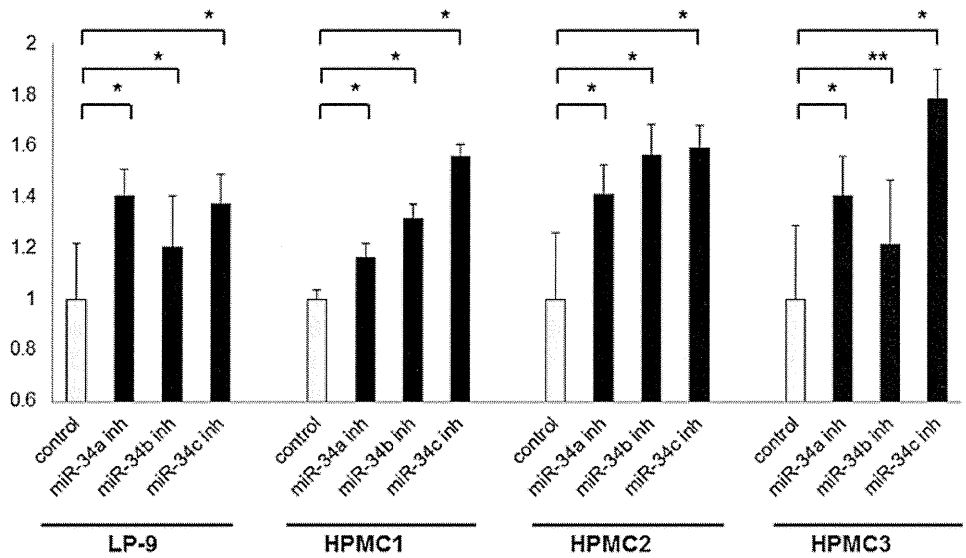

Figure 1. Effects of the inhibition of miR-34s on cell viability were evaluated using MTS assays. Control, scramble control; miR-34a, miR-34b and miR-34c inh indicate anti-miR-34a, anti-miR-34b and anti-miR-34c inhibitors. HPMC, human primary-cultured mesothelial cell. Values are expressed as the means ± SD of three experiments. *P<0.01, **P=0.01.

SDS-PAGE and was then transferred to PVDF membranes. The proteins on the membranes were incubated overnight at 4˚C with the primary antibodies. The primary antibodies used for western blotting were as follows: anti-MET (25H2; Cell Signaling), anti-phospho-MET (3D7, Tyr1234/1235; Cell Signaling) and anti-bcl-2 (human specific; Cell Signaling). The following secondary antibodies were used: goat anti-rabbit or anti-mouse IgG-conjugated horseradish peroxidase (Santa Cruz Biotechnology, Santa Cruz, CA). To detect the specific signals, the membranes were examined using ECL Plus Western Blotting Detection reagents (Amersham Biosciences UK Ltd., Buckinghamshire, UK).

Statistical analysis. The statistical analysis was performed using SPSS for Windows version 17.0 (SPSS Inc., Chicago, IL, USA). All of the *in vitro* experiments were performed at least three times. Data are represented as the means ± standard deviation. The significance of the differences between the two groups was determined using the Chi-square test and the Mann-Whitney U-test, as appropriate. A 5% significance level (P<0.05) was considered to indicate a statistically significant result.

Results

miR-34 inhibition by transfection with miR-34 inhibitors. We transfected the LP-9 cells and HPMCs with a scramble control and miR-34 inhibitors and confirmed that the expression of the miR-34s was suppressed in all of the cells, compared with the scramble control, using a real-time PCR method: 80-89% inhibition for the miR-34a inhibitor, 45-73% for miR-34b and 68-70% for miR-34c.

Impact of miR-34 inhibitors on cell viability and proliferation. To screen for the cell viability effect of miR-34 inhibition, we performed MTS assays in LP-9 cells and the three mesothelial cell lines using transient transfection. miR-34a, -34b and -34c inhibitors significantly increased the cell viability of all the examined cells, compared with the scramble control (1.2- to 1.4-fold for miR-34a, 1.2- to 1.6-fold for miR-34b, and 1.4- to 1.8-fold for miR-34c) (Fig. 1). In addition, to screen for the cell proliferation potential of miR-34 inhibition, we performed a colony formation assay and investigated the expression of Ki-67 in the LP-9 cells. The number of visible colonies was significantly increased in the cells transfected with the miR-34 inhibitors, compared with the scramble control (Fig. 2). The number of Ki-67-stained cells was significantly increased in cells transfected with the miR-34a (P<0.01) and -34c (P<0.01) inhibitors, compared with the scramble control. However, cells transfected with the miR-34b inhibitor tended to have increased numbers of Ki-67-stained cells (P=0.09) (Fig. 3). Regarding the anchorage-independent growth potential of miR-34 inhibition, LP-9 cells transfected with both the scramble control and miR-34 inhibitors did not grow in soft agar.

Impact of miR-34 inhibitors on migration and invasion. Cell migration and invasion potential were examined using a Boyden chamber. Microscopy images of the Boyden chamber assay are shown in Fig. 4. Both migration and invasion were significantly increased in the LP-9 cells transfected with all miR-34 inhibitors (P<0.01), compared with the scramble control. Parental HPMCs did not exhibit migration or invasion in this study, and such features were not acquired after transfection with miR-34 inhibitors.

Cell cycle analysis of LP-9 cells transfected with miR-34 inhibitors. Cell cycle analysis was conducted for LP-9 cells transfected with the scramble control or miR-34 inhibitors. The LP-9 cells transfected with the miR-34 inhibitors showed a slight decrease in the G0-G1 cell fraction, indicating that miR-34 inhibitors reduced G1 arrest (2.0-4.6% decrease for miR inhibitors) (data not shown).

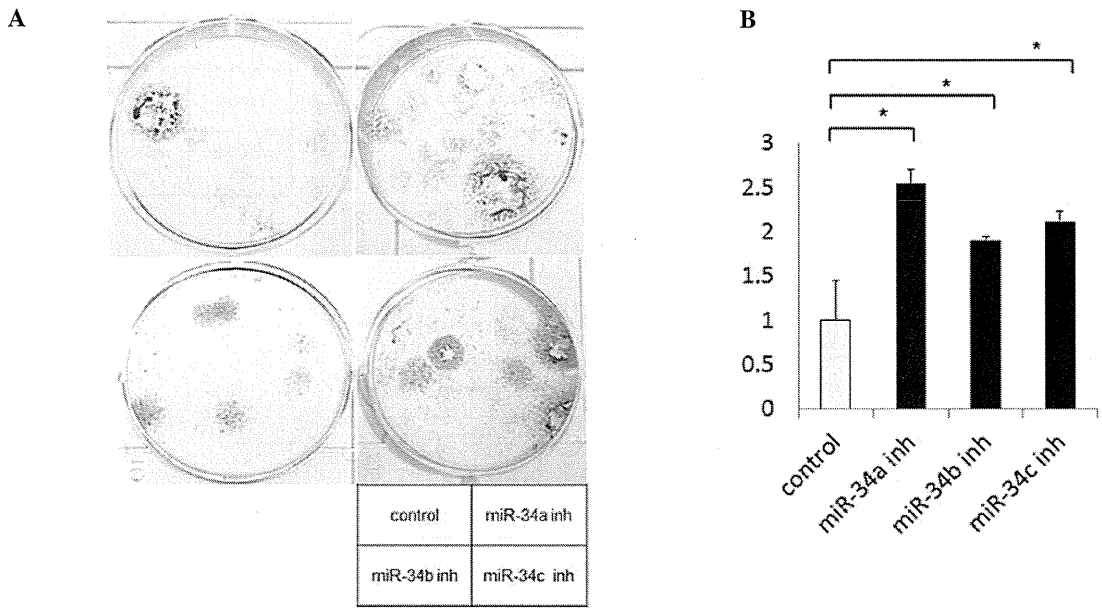

Figure 2. Effects of the inhibition of miR-34s on cell proliferation were evaluated using a colony formation assay in LP-9 cells. (A) Representative images of colony formation assay. (B) The number of colonies in control was set as 1 and the number of colonies in the treated cells was compared. Control, scramble control; miR-34a, miR-34b and miR-34c inh indicate anti-miR-34a, anti-miR-34b and anti-miR-34c inhibitors. Values are expressed as the means ± SD of three experiments. *P<0.01.

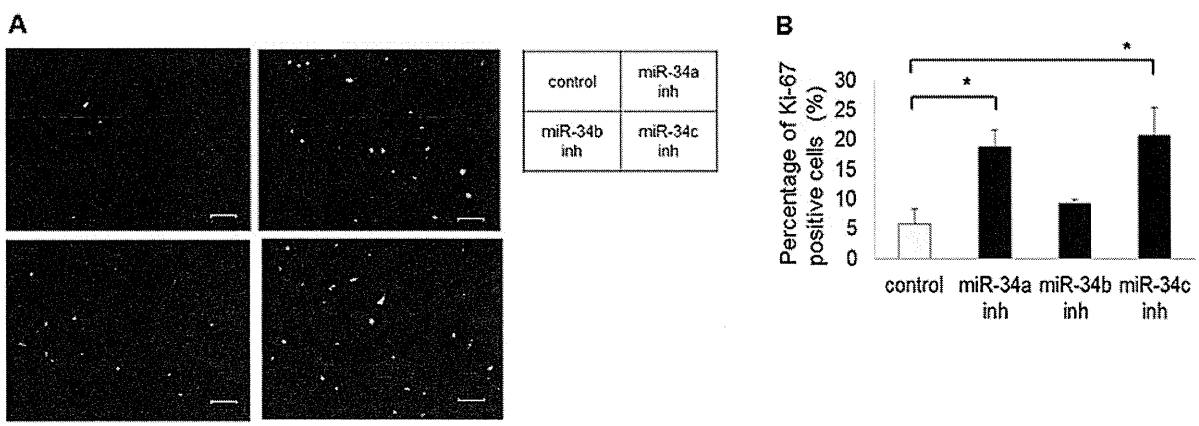

Figure 3. Effects of the inhibition of miR-34s on the immunofluorescent analysis of Ki-67 protein in LP-9 cells. (A) Representative images of immunofluorescent staining of Ki-67. Scale bars, 100 μm. (B) The percentage of Ki-67-positive cells in the treated cells was compared with that of the control. Control, scramble control; miR-34a, miR-34b and miR-34c inh indicate anti-miR-34a, anti-miR-34b and anti-miR-34c inhibitors. Values are expressed as the means ± SD of three microscopic fields. *P<0.01.

Protein expression of LP-9 cells transfected with miR-34 inhibitors. To examine the effect of miR-34 inhibition, we focused on c-MET (both total and phosphorylated types) and Bcl-2, which are putative targets of miR-34s. Western blotting was performed using LP-9 cells transfected with the scramble control or miR-34 inhibitors. The total and phosphorylated c-MET and Bcl-2 expression levels were upregulated in the LP-9 cells transfected with the miR-34 inhibitors (Fig. 5).

Discussion

In the present study, we found that the downregulation of miR-34s in human mesothelial cells prompted increased cell viability, proliferation, resistance to apoptosis, and invasive potential but failed to increase anchorage-independent growth potential. We previously reported that the epigenetic silencing of miR-34b/c by methylation was extremely common (100% of cell lines) and played an important role in the tumorigenesis of MM. In that study, miR-34a was also found to be downregulated by methylation (30% of cell lines), suggesting a tumorigenic role in MM (10). Of note, Ji *et al* (14) reported that the restoration of miR-34s significantly inhibited clonogenic growth, while the inhibition of endogenous miR-34s by miR-34 inhibitors promoted growth in human pancreatic cancer cell lines. These results suggest that the inhibition of miR-34s is an important factor contributing to MM carcinogenesis.

Regarding the study of the oncogenic transformation of normal cells, the introduction of oncogenes, such as *K-RAS*

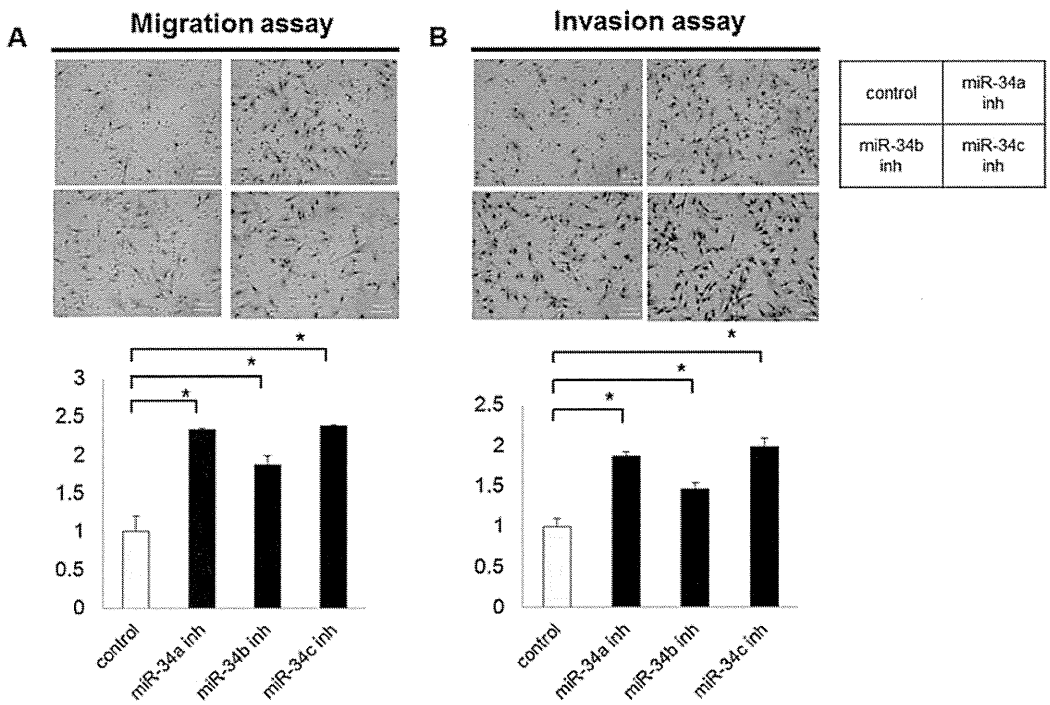

Figure 4. Effects of the inhibition of miR-34s on migration and invasive potential using migration (A) or invasion (B) assays in LP-9 cells. Control, scramble control; miR-34a, miR-34b and miR-34c inh indicate anti-miR-34a, anti-miR-34b and anti-miR-34c inhibitors. The quantitative values expressed as the means ± SD of five microscopic fields are representative of three experiments. Scale bars, 100 μm. *P<0.01.

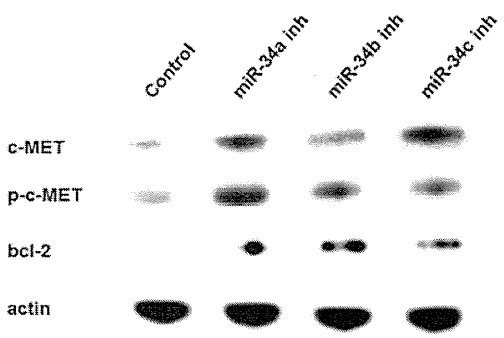

Figure 5. Effects of the inhibition of miR-34s on the protein expression profile of c-MET, p-c-MET and bcl-2 in LP-9 cells. Control, scramble control; miR-34a, miR-34b and miR-34c inh indicate anti-miR-34a, anti-miR-34b and anti-miR-34c inhibitors.

or *HRAS* and *c-MYC*, caused the induction of a malignant phenotype in human bronchial epithelial cells (15-17). Sato *et al* (18) also reported that additional genetic changes, such as p53 knockdown, *K-RAS*^{V12}, and mutant epidermal growth factor receptor (EGFR), either alone or in combination, caused the progression of human bronchial epithelial cells at least partly toward malignancy, including the development of characteristics such as a higher saturation density, anchorage-independent growth, and an invasive phenotype, but failed to induce tumor formation. In our study, miR-34 inhibition induced increased cell viability in all the human mesothelial cell lines, and increased cell proliferation and invasive potential in LP-9 cells. However, miR-34 inhibition failed to promote anchorage-independent growth potential, suggesting that the inhibition of miR-34s was not only sufficient to cause crude mesothelial cells to undergo apparent malignant transformation but that other molecular alterations are required for the carcinogenic process in human mesothelial cells. Analysis of the immunofluorescent staining of Ki-67 demonstrated that cells transfected with miR-34a and -34c inhibitors exhibited significantly increased numbers of Ki-67-positive stained cells, compared with the scramble control, although the cells transfected with the miR-34b inhibitor did not. The absence of significant differences in the miR-34b inhibitor suggest that the inhibition efficiency of the miR-34b inhibitor was lower than that of the miR-34a and 34c inhibitors in this study.

Several genes have been identified as targets of the miR-34s (9). In this study, *c-MET* and *Bcl-2* genes were examined as these gene products are considered to be important molecules in MM and were upregulated after miR-34 inhibition. c-MET was found to be activated in MM through overexpression or mutation, and its ligand, hepatocyte growth factor, was found to be overexpressed in MMs (19). Indeed, the suppression of c-MET using MET inhibitors revealed a potent inhibition of proliferation, invasion and migration in several MM cell lines (20). Bcl-2 is an anti-apoptotic protein located downstream of p53. The overexpression of Bcl-2 in MM has been reported in immunohistochemical analysis (21,22) and is considered to be responsible for the anti-apoptotic feature of MM. Considering the results of western blot analysis together with colony formation assay and cell cycle analysis, our findings suggest that the inhibition of miR-34s increases the grade of malignancy in mesothelial cells through c-MET and Bcl-2.

In conclusion, the present study, together with the findings of our previous report, strongly suggest that miR-34s play an important role in the early carcinogenic progression of human mesothelial cells to malignant mesothelioma.

Acknowledgements

We thank the Central Research Laboratory of the Okayama University Medical School for the technical support for the immunohistochemical staining. This study was supported by Grant-in-Aids for Scientific Research from the Ministry of Education, Culture, Sports, Science and Technology of Japan 22591566 (S.T.).

References

1. Robinson BW and Lake RA: Advances in malignant mesothelioma. N Engl J Med 353: 1591-1603, 2005.
2. Jakobsen JN and Sorensen JB: Review on clinical trials of targeted treatments in malignant mesothelioma. Cancer Chemother Pharmacol 68: 1-15, 2011.
3. Hansen J, de Klerk NH, Musk AW and Hobbs MS: Environmental exposure to crocidolite and mesothelioma: exposure-response relationships. Am J Respir Crit Care Med 157: 69-75, 1998.
4. Toyooka S, Kishimoto T and Date H: Advances in the molecular biology of malignant mesothelioma. Acta Med Okayama 62: 1-7, 2008.
5. Croce CM and Calin GA: miRNAs, cancer, and stem cell division. Cell 122: 6-7, 2005.
6. Hatfield S and Ruohola-Baker H: microRNA and stem cell function. Cell Tissue Res 331: 57-66, 2008.
7. Zhang W, Dahlberg JE and Tam W: MicroRNAs in tumorigenesis: a primer. Am J Pathol 171: 728-738, 2007.
8. He L, He X, Lim LP, *et al*: A microRNA component of the p53 tumour suppressor network. Nature 447: 1130-1134, 2007.
9. Hermeking H: p53 enters the microRNA world. Cancer Cell 12: 414-418, 2007.
10. Kubo T, Toyooka S, Tsukuda K, *et al*: Epigenetic silencing of microRNA-34b/c plays an important role in the pathogenesis of malignant pleural mesothelioma. Clin Cancer Res 17: 4965-4974, 2011.
11. Carbone M, Rizzo P, Grimley PM, *et al*: Simian virus-40 large-T antigen binds p53 in human mesotheliomas. Nat Med 3: 908-912, 1997.
12. Shimamura A and Fisher DE: p53 in life and death. Clin Cancer Res 2: 435-440, 1996.
13. Toyooka S, Pass HI, Shivapurkar N, *et al*: Aberrant methylation and simian virus 40 tag sequences in malignant mesothelioma. Cancer Res 61: 5727-5730, 2001.
14. Ji Q, Hao X, Zhang M, *et al*: MicroRNA miR-34 inhibits human pancreatic cancer tumor-initiating cells. PLoS One 4: e6816, 2009.
15. Reddel RR, Ke Y, Kaighn ME, *et al*: Human bronchial epithelial cells neoplastically transformed by v-Ki-ras: altered response to inducers of terminal squamous differentiation. Oncogene Res 3: 401-408, 1988.
16. Ura H, Bonfil RD, Reich R, *et al*: Expression of type IV collagenase and procollagen genes and its correlation with the tumorigenic, invasive, and metastatic abilities of oncogene-transformed human bronchial epithelial cells. Cancer Res 49: 4615-4621, 1989.
17. Yoakum GH, Lechner JF, Gabrielson EW, *et al*: Transformation of human bronchial epithelial cells transfected by Harvey ras oncogene. Science 227: 1174-1179, 1985.
18. Sato M, Vaughan MB, Girard L, *et al*: Multiple oncogenic changes (K-RAS(V12), p53 knockdown, mutant EGFRs, p16 bypass, telomerase) are not sufficient to confer a full malignant phenotype on human bronchial epithelial cells. Cancer Res 66: 2116-2128, 2006.
19. Harvey P, Warn A, Newman P, Perry LJ, Ball RY and Warn RM: Immunoreactivity for hepatocyte growth factor/scatter factor and its receptor, met, in human lung carcinomas and malignant mesotheliomas. J Pathol 180: 389-394, 1996.
20. Jagadeeswaran R, Ma PC, Seiwert TY, *et al*: Functional analysis of c-Met/hepatocyte growth factor pathway in malignant pleural mesothelioma. Cancer Res 66: 352-361, 2006.
21. Soini Y, Kinnula V, Kaarteenaho-Wiik R, Kurttila E, Linnainmaa K and Paakko P: Apoptosis and expression of apoptosis regulating proteins bcl-2, mcl-1, bcl-X, and bax in malignant mesothelioma. Clin Cancer Res 5: 3508-3515, 1999.
22. O'Kane SL, Pound RJ, Campbell A, Chaudhuri N, Lind MJ and Cawkwell L: Expression of Bcl-2 family members in malignant pleural mesothelioma. Acta Oncol 45: 449-453, 2006.

Invest New Drugs
DOI 10.1007/s10637-013-9941-z

PHASE II STUDIES

Pemetrexed and carboplatin followed by pemetrexed maintenance therapy in chemo-naïve patients with advanced nonsquamous non-small-cell lung cancer

Isamu Okamoto · Keisuke Aoe · Terufumi Kato · Yukio Hosomi · Akira Yokoyama · Fumio Imamura · Katsuyuki Kiura · Tomonori Hirashima · Makoto Nishio · Naoyuki Nogami · Hiroaki Okamoto · Hideo Saka · Nobuyuki Yamamoto · Naoto Yoshizuka · Risa Sekiguchi · Kazuhiro Kiyosawa · Kazuhiko Nakagawa · Tomohide Tamura

Received: 13 November 2012 / Accepted: 19 February 2013

Summary *Introduction* This study prospectively evaluated the efficacy and safety of pemetrexed and carboplatin followed by maintenance pemetrexed in chemo-naïve patients with advanced nonsquamous non-small cell lung cancer (NSCLC). *Methods* A total of 109 patients received pemetrexed (500 mg/m^2) and carboplatin (area under the curve = 6 mg/mL·min) every 21 days. For patients without disease progression after 4 cycles, pemetrexed was continued until disease progression or unacceptable toxicity. Pre-planned subgroup analysis results based on the presence of epidermal growth factor receptor (*EGFR*) mutations are also presented. *Results* The median number of treatment cycles was 5 (range: 1–30) in the entire study period. Most of the grade ≥3 toxicities observed were hematologic in nature, with no increase in

This study is registered with ClinicalTrials.gov. identifier NCT01020786
Funding source: This trial is sponsored by Eli Lilly Japan K.K.

I. Okamoto (✉) · K. Nakagawa
Department of Medical Oncology,
Kinki University Faculty of Medicine, 377-2 Ohno-higashi,
Osaka-Sayama, Osaka 589-8511, Japan
e-mail: chi-okamoto@dotd.med.kindai.ac.jp

K. Aoe
National Hospital Organization Yamaguchi-Ube Medical Center,
Yamaguchi, Japan

T. Kato
Kanagawa Cardiovascular and Respiratory Center, Kanagawa, Japan

Y. Hosomi
Tokyo Metropolitan Cancer and Infectious Diseases Center
Komagome Hospital, Tokyo, Japan

A. Yokoyama
Niigata Cancer Center Hospital, Niigata, Japan

F. Imamura
Osaka Medical Center for Cancer and Cardiovascular Diseases,
Osaka, Japan

K. Kiura
Okayama University Hospital, Okayama, Japan

T. Hirashima
Osaka Prefectural Medical Center for Respiratory
and Allergic Diseases, Osaka, Japan

M. Nishio
Cancer Institute Hospital of Japanese Foundation for Cancer
Research, Tokyo, Japan

N. Nogami
National Hospital Organization Shikoku Cancer Center,
Ehime, Japan

H. Okamoto
Yokohama Municipal Citizen's Hospital, Kanagawa, Japan

H. Saka
National Hospital Organization Nagoya Medical Center,
Aichi, Japan

N. Yamamoto
Shizuoka Cancer Center, Shizuoka, Japan

N. Yoshizuka · R. Sekiguchi · K. Kiyosawa
Eli Lilly Japan K.K., Hyogo, Japan

T. Tamura
National Cancer Center Hospital, Tokyo, Japan

Published online: 10 March 2013

the relative incidence associated with continuation maintenance therapy with pemetrexed. Among the 106 total patients assessable for efficacy, the objective response rate was 35.8 %, median progression free survival (PFS) 5.7 months, and median overall survival (OS) 20.2 months. Sixty patients received maintenance pemetrexed (median: 4 cycles, range: 1–26 cycles); median PFS from the beginning of induction treatment was 7.5 months. From the subgroup analysis for *EGFR* mutation status, the median OS of *EGFR* wild-type patients (n=61) was 20.2 months. *Conclusions* Pemetrexed/carboplatin followed by pemetrexed was well tolerated and active for front-line treatment of advanced nonsquamous NSCLC. Encouraging survival outcomes were observed even in *EGFR*-wild type patients.

Keywords Pemetrexed · Carboplatin · Continuation maintenance · Nonsquamous NSCLC · *EGFR* mutation status

Introduction

Lung cancer is the most common type of cancer globally and the leading cause of cancer death [1]. Approximately 85 % of patients with lung cancer have non-small cell lung cancer (NSCLC), and 70 % of NSCLC is inoperable, locally advanced, or metastatic [2]. Currently, nonsquamous histology has been an important determinant for clinical outcome in NSCLC patients treated with pemetrexed or bevacizumab chemotherapy [3–8]. In addition, oncogenic driver mutations, such as *EGFR* mutation and fusions of echinoderm microtubule-associated protein-like 4 (EML4) and anaplastic lymphoma kinase (ALK), were found in a subset of patients with nonsquamous NSCLC. A higher proportion of tumors harboring *EGFR* mutations were reported in East Asian compared with Caucasian patients [9]. While some molecular-targeted agents, such as gefitinib, erlotinib and crizotinib, have dramatically improved overall survival in the population harboring these targetable oncogenic gene alterations, prognosis of the other wild-type patients with NSCLC remains to be improved [10–16].

Pemetrexed, a potent multitargeted antifolate, inhibits thymidylate synthase, dihydrofolate reductase, and glycinamide ribonucleotide formyltransferase, all of which are involved in the *de novo* synthesis of purines or pyrimidines [17]. Pemetrexed is the key drug in the treatment for nonsquamous NSCLC patients, showing consistently superior efficacy compared with standard treatments [4–7]. Recently, a new treatment paradigm using pemetrexed for continuation maintenance therapy after 4 cycles of pemetrexed/cisplatin has been reported in a large phase III trial [18]. Continuation maintenance therapy with pemetrexed improved PFS and OS in patients with advanced nonsquamous NSCLC compared with placebo.

While pemetrexed/cisplatin followed by pemetrexed maintenance therapy is the standard treatment in nonsquamous NSCLC, carboplatin-based regimens have been widely used as a substitute for cisplatin-based regimens due to their lower toxicity and more convenience for administering in outpatient treatment settings. However, clinical outcomes of continuation therapy with pemetrexed following pemetrexed in combination with carboplatin have not fully been addressed. This study was conducted to evaluate efficacy, including the survival outcome and safety of pemetrexed/carboplatin combination therapy followed by continuation maintenance with pemetrexed in chemo-naïve patients with advanced nonsquamous NSCLC. Given that *EGFR* mutation status has recently become a key factor for the overall treatment plan of advanced NSCLC, we also assessed the efficacy data according to the *EGFR* mutation status using a pre-planned analysis.

Materials and methods

Eligibility

Patients 20 years of age or older with histologically or cytologically confirmed advanced NSCLC, other than predominantly squamous cell histology, were eligible for the study. Each patient was required to have clinical stage IIIB, stage IV or recurrent disease, a lesion not amenable to curative radiation, and no history of prior chemotherapy [19]. Eligibility stipulated an Eastern Cooperative Oncology Group (ECOG) performance status of 0 or 1, and adequate function of the lungs, bone marrow, liver, and kidneys. The criteria for organ function specified baseline resting arterial oxygen saturation (SpO_2) on room air ≥93 %; hemoglobin ≥9.0 g/dL, white blood cells ≥3000/mm^3, neutrophils ≥1500/mm^3, platelets ≥100,000/mm^3, aspartate aminotransferase (AST)/alanine aminotransferase (ALT) ≤2.5 times upper limit of normal (ULN), total bilirubin ≤1.5 times ULN, creatinine ≤1.5 times ULN, and 24-h creatinine clearance or calculated creatinine clearance ≥45 mL/min as estimated by the Cockcroft and Gault formula. Patients were required to have a life expectancy of at least 12 weeks and no brain metastases other than stable, asymptomatic, or treated metastatic brain tumors. This study was conducted following good clinical practices and the ethical principles outlined in the Declaration of Helsinki. This study protocol was approved by the institutional review board at each participating center. All patients signed written informed consent before enrollment. The trial has been registered under the number NCT 01020786.

Study design and treatment

This was an open-label, multicenter, single arm, prospective postmarketing study. The primary objective was to evaluate

the efficacy, as measured by PFS, of this study treatment in patients with advanced nonsquamous NSCLC who received at least one dose of the initial combination therapy. Secondary endpoints, including OS, disease control rate (DCR), overall response rate (ORR), and safety, were also evaluated.

Eligible patients received pemetrexed 500 mg/m^2 through a 10-min intravenous infusion followed by intravenous infusion of carboplatin at a dose corresponding to target area under the curve (AUC) equal to 6 mg/mL·min (AUC6) over at least 30 min on day 1. This combination therapy was repeated every 21 days for up to 4 cycles. After 4 cycles, patients with complete response (CR), partial response (PR), or stable disease (SD) received maintenance therapy with pemetrexed 500 mg/m^2 every 21 days until evidence of disease progression or development of unacceptable toxicities. All patients received oral folic acid (0.5 mg) daily and a vitamin B_{12} (1 mg) injection every 9 weeks, beginning at least 1 week before the first dose and continuing until 3 weeks after the last dose of study treatment.

Subsequent cycles of treatment were withheld until the following criteria were satisfied: neutrophil count ≥1500/mm^3, platelet count ≥100,000/mm^3, hemoglobin ≥8.0 g/dL, ECOG performance status ≤1, SpO_2 ≥93 %, AST/ALT ≤2.5 times ULN, total bilirubin ≤1.5 times ULN, and 24-h creatinine clearance or calculated creatinine clearance ≥45 mL/min as estimated by the Cockcroft and Gault formula, other tolerable nonhematologic toxicity, and a decision by the physician. If these criteria were not satisfied within 29 days from the date of dose administration in the cycle because of adverse events, the pemetrexed dose was reduced from 500 to 400 mg/m^2 or from 400 to 300 mg/m^2, and the carboplatin dose was reduced from AUC6 to an AUC of 5 mg/mL·min (AUC5) or from AUC5 to an AUC of 4 mg/mL·min (AUC4). Any patient who required a third dose reduction was withdrawn from the study. In addition, if the next cycle had not started within 43 days from previous dosing due to toxicity, the patient was discontinued.

Baseline and treatment assessments

Baseline evaluations included medical history, physical examination, electrocardiogram, tumor status, ECOG performance status, clinical laboratory test, and *EGFR* mutation status. Testing for *EGFR* mutations was outsourced from each institution to commercial clinical laboratories in Japan. Computed tomography was performed for tumor assessment within 21 days of initiation of study treatment and was repeated every 6 weeks thereafter. All responses were defined according to Response Evaluation Criteria in Solid Tumors (RECIST) criteria, version 1.0. If a patient was documented as having a CR or a PR, a confirmatory evaluation was performed after an interval of at least 4 weeks. The patient was considered to have SD if it was confirmed and sustained for 6 weeks or longer after the start of study treatment. PFS was defined as the time from enrollment to the date of confirmation of progressive disease (PD) or the date of death from any cause (whichever occurs earlier). Patients who received any subsequent systemic anticancer therapy prior to objective PD or death would be censored at the date of the last objective progression-free disease assessment prior to starting the subsequent systemic anticancer therapy. Overall survival was defined as the time from enrollment until death from any cause. For patients with unknown death status, OS would be censored at the last date the patient was known to still be alive.

Toxicities were graded according to the National Cancer Institute Common Terminology Criteria for Adverse Events, version 3.0.

Statistical methods

The sample size of 100 patients had a power of 90 % at a one-sided type I error rate of 0.05 to compare PFS of this study regimen versus the first-line platinum-based combination therapy as a constant value under the following assumptions: the expected PFS of the first-line therapy of platinum-based combination regimen was 5 months, the expected PFS of this study treatment was 7 months, the enrollment period was 8 months, and the follow-up period was 12 months.

Efficacy and safety analyses were planned to be performed on patients who received at least one dose of the treatment. Since some patients had significant protocol violations during the study, they were excluded from the efficacy analysis prior to the database lock. In this manuscript, the efficacy was assessed on the latter data set.

Time-to-event variables were analyzed using Kaplan-Meier estimation techniques, including Kaplan-Meier curves, quartiles, and interval estimation using 90 % and 95 % confidence intervals (CIs). For DCR and ORR, 95 % CIs were calculated using the exact test. Prespecified subgroup analyses for PFS and ORR based on *EGFR* mutation status were also included.

Results

Patient characteristics

Patient disposition is shown in Fig. 1. Between December 2009 and July 2010, 111 patients with recurrent or newly diagnosed, advanced nonsquamous NSCLC were enrolled at 25 clinical sites in Japan. Two patients were subsequently discontinued from the study for not meeting entry criteria, and 109 patients received the study treatment. Baseline characteristics are summarized in Table 1. The median age for the treated population was 63 years (range: 38–78 years), and 40 patients (36.7 %) were female. Other key characteristics at baseline included